

Dalton Transactions

Accepted Manuscript



This is an *Accepted Manuscript*, which has been through the Royal Society of Chemistry peer review process and has been accepted for publication.

Accepted Manuscripts are published online shortly after acceptance, before technical editing, formatting and proof reading. Using this free service, authors can make their results available to the community, in citable form, before we publish the edited article. We will replace this *Accepted Manuscript* with the edited and formatted *Advance Article* as soon as it is available.

You can find more information about *Accepted Manuscripts* in the [Information for Authors](#).

Please note that technical editing may introduce minor changes to the text and/or graphics, which may alter content. The journal's standard [Terms & Conditions](#) and the [Ethical guidelines](#) still apply. In no event shall the Royal Society of Chemistry be held responsible for any errors or omissions in this *Accepted Manuscript* or any consequences arising from the use of any information it contains.

ARTICLE

Halogen-Bonding in a New Family of tris(haloanilato)metallate(III) Magnetic Molecular Building Blocks

Cite this: DOI: 10.1039/x0xx00000x

Received 00th January 2012,
Accepted 00th January 2012

DOI: 10.1039/x0xx00000x

www.rsc.org/

Matteo Atzori,[†] Flavia Artizzu,[†] Elisa Sessini,[†] Luciano Marchiò,[‡] Danilo Loche,[†] Angela Serpe,[†] Paola Deplano,[†] Giorgio Concas,[§] Flavia Pop,[◇] Narcis Avarvari,[◇] and Maria Laura Mercuri^{†,*}

Here we report on new tris(haloanilato)metallate(III) complexes with general formula $[A]_3[M(X_2An)_3]$ ($A = (n-Bu)_4N^+$, $(Ph)_4P^+$; $M = Cr(III)$, $Fe(III)$; $X_2An = 3,6$ -dihalo derivatives of 2,5-dihydroxybenzoquinone ($H_4C_6O_4$), chloranilate (Cl_2An^{2-}), bromanilate (Br_2An^{2-}) and iodanilate (I_2An^{2-})), obtained by a general synthetic strategy, and their full characterization. The crystal structures of these $Fe(III)$ and $Cr(III)$ haloanilate complexes consist of anions formed by homoleptic complexes formulated as $[M(X_2An)_3]^{3-}$ and $(Et)_3NH^+$, $(n-Bu)_4N^+$, or $(Ph_4)P^+$ cations. All complexes exhibit octahedral coordination geometry with metal ions surrounded by six oxygen atoms from three chelate ligands. These complexes are chiral according to the metal coordination of three bidentate ligands, and both Λ and Δ enantiomers are present in their crystal lattice. The packing of $[(n-Bu)_4N]_3[Cr(I_2An)_3]$ (**5a**) shows that the complexes form supramolecular dimers that are held together by two symmetry related $I \cdots O$ interactions (3.092(8) Å), considerably shorter than the sum of iodine and oxygen van der Waals radii (3.50 Å). The $I \cdots O$ interaction can be regarded as a halogen bond (XB), where the iodine behaves as XB donor and the oxygen atom as the XB acceptor. This is in agreement with the properties of the electrostatic potential for $[Cr(I_2An)_3]^{3-}$ that predicts a negative charge accumulation on the peripheral oxygen atoms and a positive charge accumulation on the iodine. The magnetic behaviour of all complexes, except the **5a**, may be explained by considering a set of paramagnetic non-interacting $Fe(III)$ or $Cr(III)$ ions, taking into account the zero-field splitting effect. The presence of strong XB interactions in **5a** are capable, instead, to promote antiferromagnetic interactions among paramagnetic centers at low temperature, as shown by the fit with the Curie-Weiss law, in agreement with the formation of halogen-bonded supramolecular dimers.

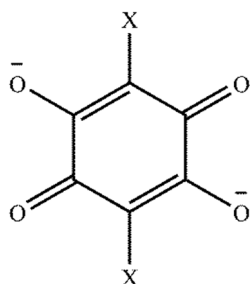
Introduction

Over the last decade halogen bonding (XB) has gained great interest for the construction of self-assembled supramolecular architectures out of the large array of known non-covalent bonds, namely hydrogen bonding, π - π and van der Waals interactions and electrostatic forces. XB which is a strong, specific and highly directional non-covalent interaction, is characterized by i) $X \cdots A$ ($A =$ acceptor) distance shorter than the sum of the van der Waals radii, ii) linearity of the $D-X \cdots A$ ($D =$ donor) bond, higher than in hydrogen bonds, iii) preferred orientation of the $D-X$ bond in the plane of the lone pair of A with a preference for the lone pair direction within that plane, and iv) tendency for stronger XB in the order $I > Br > Cl$.¹ This interaction can be as effective as hydrogen bonding (HB) for driving highly specific crystal packing motifs but, while applications of HB in various research areas such as materials

science and synthetic chemistry are abundant,² the development of halogen bonded systems is still in its infancy. XB has been introduced very successfully in 1995 in the field of molecular conductors by Imakubo and Kato for controlling the solid-state organization of radical cation salts of iodotetrathiafulvalenes such as EDT-TTF-I (iodo-ethylene-dithio-tetrathiafulvalene) with counterions of Lewis base character such as Br^- , $Ag(CN)^{2-}$, etc.,³ moreover these interactions have been observed in neutral halogenated tetrathiafulvalenes as well as in their radical cation salts. Fourmigué and Batail have reported exhaustively on the use of directional, electrostatic, normal, and weak hydrogen bonds and halogen bonds intermolecular interactions in crystalline molecular conductors based on functionalized tetrathiafulvalene (TTF) derivatives.⁴

In the search for novel halogen-bonded systems where the halogen atom can play a multifunctional role, either at the

electronic or at the supramolecular level, on the physical properties of supramolecular systems that stem from specific XB-oriented organizations, we focused our attention on the 3,6-dihalo derivatives of 2,5-dihydroxybenzoquinone ($\text{H}_4\text{C}_6\text{O}_4$), chloranilate ($\text{C}_6\text{O}_4\text{Cl}_2^{2-}$, hereafter $\text{Cl}_2\text{An}^{2-}$), bromanilate ($\text{C}_6\text{O}_4\text{Br}_2^{2-}$, hereafter $\text{Br}_2\text{An}^{2-}$) and iodanilate ($\text{C}_6\text{O}_4\text{I}_2^{2-}$, hereafter I_2An^{2-}) (Scheme 1), as promising building blocks of the above-mentioned molecule-based materials.



Scheme 1 Molecular structures for the chloranilate ($\text{X} = \text{Cl}$), bromanilate ($\text{X} = \text{Br}$), and iodanilate ($\text{X} = \text{I}$) dianions.

The coordination chemistry of these ligands is described in literature with particular attention for the chloranilate one.⁵ Among the haloanilato-complexes, some dinuclear⁶ and several n -D ($n = 1, 2, 3$) polymeric systems have been reported,⁷ but only few examples of mononuclear complexes have been obtained so far.^{8,6a} To the best of our knowledge, except the tris(chloranilato)ferrate(III) complex obtained by Miller *et al.* as counteranion of a Fe(III) cationic dimeric complex,⁹ no reports on the synthesis and characterization of tris-chelated homoleptic mononuclear complexes with the previously mentioned ligands are available in the literature so far. We report herein the synthesis and full characterization of six new tris(haloanilato)metallate(III) complexes with general formula $[\text{A}]_3[\text{M}(\text{X}_2\text{An})_3]$ ($\text{M} = \text{Cr}(\text{III}), \text{X} = \text{Cl}$ (**1**), Br (**3**), I (**5**); $\text{M} = \text{Fe}(\text{III}), \text{X} = \text{Cl}$ (**2**), Br (**4**), I (**6**); $\text{A} = (n\text{-Bu})_4\text{N}^+$ (**1a-6a**), $(\text{Ph})_4\text{P}^+$ (**1b-6b**), $(\text{Et})_3\text{NH}^+$ (**1c-2c**)) (see Chart 1) which have been used as suitable building units for the preparation of novel molecule-based magnets and metal-organic frameworks (MOFs).¹⁰ In these systems the nature of the halogen atom plays a crucial role in determining their physical properties. In fact, very recently some of us reported on a strategy to control the magnetic properties of a new family of layered chiral porous molecular magnets formulated as $\text{A}[\text{M}^{\text{II}}\text{Cr}^{\text{III}}(\text{X}_2\text{An})_3]\cdot\text{G}$, where a simple change in the halogen atom (X) allows for a fine tuning of the magnetic properties so that the ordering temperature increases from 5.5 to 6.3 and 8.2 K for $\text{X} = \text{Cl}, \text{Br}, \text{I}$ respectively.¹⁰ Furthermore, since these materials crystallize in an eclipsed honeycomb structure, they present hexagonal channels with a void volume of ca. 20 % that can be filled with guest molecules (G) and they may have the potential to behave as a new family of metal-organic frameworks (MOFs), where the halogen size can tune the dimensions of the channels. The role of the halogen atoms in these mononuclear metal complexes as potential sources of halogen bonding interactions, studied by DFT calculations, together with a full description of

their crystal structures and their magnetic properties, will be discussed in this paper.

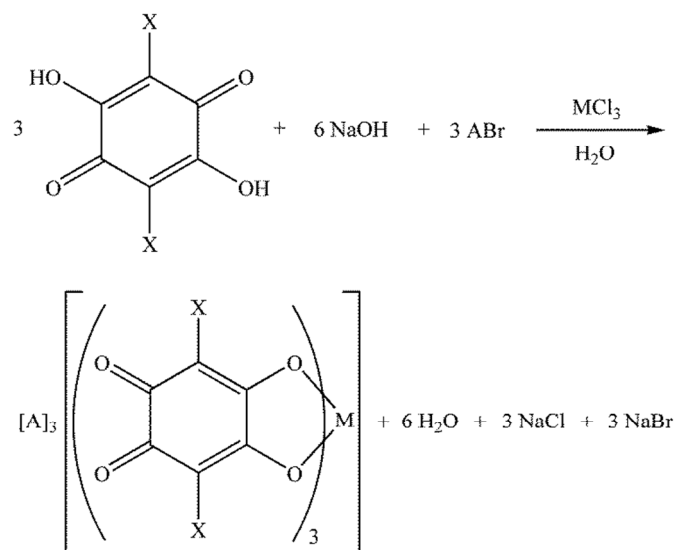
Chart 1

	$\text{Cl}_2\text{An}^{2-}$		$\text{Br}_2\text{An}^{2-}$		I_2An^{2-}	
	Cr(III)	Fe(III)	Cr(III)	Fe(III)	Cr(III)	Fe(III)
$(n\text{-Bu})_4\text{N}^+$	1a	2a	3a	4a	5a	6a
$(\text{Ph})_4\text{P}^+$	1b	2b	3b	4b	5b	6b
$(\text{Et})_3\text{NH}^+$	1c	2c	-	-	-	-

Results and Discussion

General Synthetic Strategy

The tris(haloanilato)metallate(III) complexes reported in this work have been obtained, as described in detail in the Experimental Section, according to Scheme 2.



Scheme 2 General reaction scheme for the synthesis of $[\text{A}]_3[\text{M}(\text{X}_2\text{An})_3]$ ($\text{A} = (n\text{-Bu})_4\text{N}^+, (\text{Ph})_4\text{P}^+$; $\text{M} = \text{Cr}(\text{III}), \text{Fe}(\text{III})$; $\text{X} = \text{Cl}, \text{Br}, \text{I}$).

A one-pot reaction between an aqueous solution of the trivalent metal ion ($\text{M} = \text{Cr}, \text{Fe}$) and an aqueous solution of the haloanilate dianion obtained *in situ*, allows to obtain compounds **1-6** in high yields ranging from 70 to 90%.

Molecular Structures

In the crystal structures of the Fe(III) and Cr(III) haloanilate complexes are present the complex anion of formula $[\text{M}(\text{X}_2\text{An})_3]^{3-}$ ($\text{M} = \text{Fe}$ and Cr ; $\text{X} = \text{Cl}, \text{Br}, \text{I}$) and either of the cations $(n\text{-Bu})_4\text{N}^+$, $(\text{Ph})_4\text{P}^+$, or $(\text{Et})_3\text{NH}^+$. The complexes exhibit octahedral geometry with the metal surrounded by six oxygen atoms from three chelate ligands. The metal complexes are chiral according to the metal coordination of three bidentate ligands, and in the crystal lattice both Λ and Δ enantiomers are present since all the space groups are centrosymmetric. In Figure 1 the molecular structure of **6b** is shown, whereas the structures of **2b** and **4b** are reported in the ESI (Figures S1-S2).

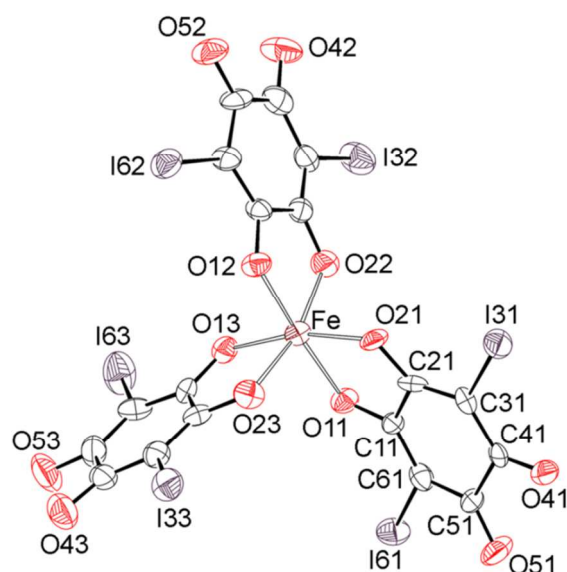
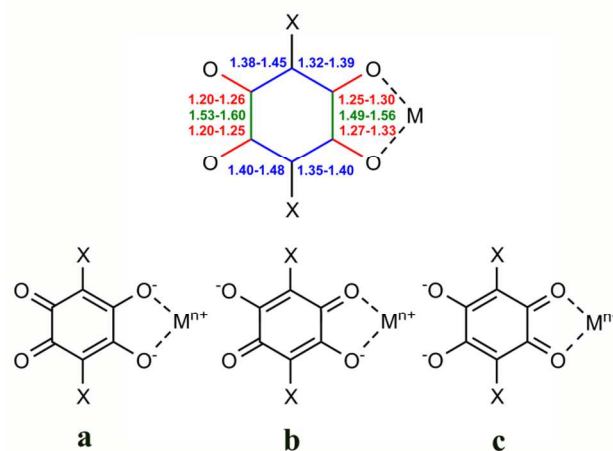


Figure 1 Ortep drawing for the anionic complex (Δ enantiomer) **6b** with thermal ellipsoids at the 30% probability level. $(\text{Ph})_4\text{P}^+$ cations and crystallization water molecules were omitted for clarity.

The metal-oxygen bond distances vary in the 1.994(7)-2.028(7) Å and 1.951(4)-1.987(4) Å ranges for the iron and chromium complexes, respectively, and are in agreement with the high spin character of these systems. Moreover the bond distances of the iron complexes are comparable with those observed in the tris(chloranilato)ferrate(III) complex obtained by Miller.⁹ The C-O bond distances are influenced by the metal coordination; in

fact, the oxygen atoms that are bound to the metal lead to C-O distances that are, on average, 0.06 Å longer than those of the peripheral oxygen atoms (see Table 1). The C-O distances are in agreement with a double bond character of the C-O moieties, whereas the OC-CO bond distances are in agreement with the presence of a single bond for all complexes (Scheme 3). In particular, according to the intra-ligand bond distances, the electronic structure of the ligand can be described as a mixture of the three limiting structures (**a**, **b** and **c**) depicted in Scheme 3, with the form **a** prevailing.



Scheme 3 Above, summary of intra-ligand bond distances (Å) ranges for **1c**, **2c**, **5a**, **2b**, **4b** and **6b** (red: C-O, green: OC-CO, and blue OC-CX distances, respectively). Below, depiction of the three limit electronic structures of the ligands. X = Cl, Br, I; M = Fe, Cr.

Table 1 Selected bond lengths (Å) for **1c**, **2c**, **5a**, **2b**, **4b**, **6b**

	1c	2c	5a	2b	4b	6b
M-O(11)	1.951(4)	1.999(2)	1.968(5)	2.002(6)	2.012(7)	2.01(1)
M-O(21)	1.972(4)	2.013(2)	1.971(4)	2.008(6)	2.020(7)	2.006(9)
M-O(12)	1.974(4)	2.003(3)	1.978(5)	2.001(6)	1.999(7)	1.99(1)
M-O(22)	1.987(4)	-	1.971(5)	2.017(6)	2.028(7)	2.00(1)
M-O(13)	1.968(4)	-	1.966(5)	2.013(6)	2.018(7)	2.04(1)
M-O(23)	1.959(4)	-	1.962(5)	1.999(6)	1.994(7)	2.01(1)
C(11)-O(11)	1.296(6)	1.275(3)	1.298(8)	1.28(1)	1.30(1)	1.30(2)
C(21)-O(21)	1.307(6)	1.279(3)	1.292(8)	1.29(1)	1.27(1)	1.29(2)
C(41)-O(41)	1.223(7)	1.216(4)	1.226(8)	1.20(1)	1.25(1)	1.22(2)
C(51)-O(51)	1.228(7)	1.229(4)	1.222(9)	1.22(1)	1.22(1)	1.20(2)
C(12)-O(12)	1.295(6)	1.280(3)	1.284(8)	1.29(1)	1.30(1)	1.33(2)
C(22)-O(22)	1.280(6)	1.227(4)	1.280(8)	1.290(9)	1.27(1)	1.30(2)
C(11)-C(21)	1.498(8)	1.519(4)	1.51(1)	1.51(1)	1.49(1)	1.56(2)
C(12)-C(22)	1.514(8)	-	1.52(1)	1.50(1)	1.51(1)	1.51(2)
C(42)-O(42)	1.230(7)	-	1.225(9)	1.23(1)	1.23(1)	1.23(2)
C(52)-O(52)	1.224(7)	-	1.207(9)	1.214(9)	1.24(1)	1.26(2)
C(13)-O(13)	1.288(6)	-	1.279(8)	1.25(2)	1.25(1)	1.33(2)
C(23)-O(23)	1.324(6)	-	1.284(8)	1.31(2)	1.30(2)	1.24(2)
C(43)-O(43)	1.236(7)	-	1.24(1)	1.23(2)	1.25(2)	1.26(2)
C(53)-O(53)	1.250(7)	-	1.245(9)	1.24(2)	1.24(2)	2.09(1)
C(31)-Cl(31)	1.748(6)	1.724(3)	2.058(7)	1.736(9)	1.88(1)	2.05(1)
C(61)-Cl(61)	1.763(6)	1.725(4)	2.088(7)	1.744(9)	1.88(1)	2.09(2)
C(32)-Cl(32)	1.745(6)	1.729(3)	2.068(8)	1.728(9)	1.88(1)	2.07(2)
C(62)-Cl(62)	1.733(6)	-	2.074(7)	1.729(9)	1.88(1)	2.09(2)
C(33)-Cl(33)	1.724(7)	-	2.053(9)	1.81(2)	1.90(2)	2.07(2)
C(63)-Cl(63)	1.726(6)	-	2.078(9)	1.80(2)	1.89(2)	1.51(2)
C(13)-C(23)	1.500(8)	1.512(6)	1.50(1)	1.52(2)	1.50(1)	1.23(2)

Symmetry code $\bar{y} = -x, y, -z+1/2$

The packing of **2c** reveals that the complex molecules exchange two types of interactions with the surrounding complexes (Figure 2).

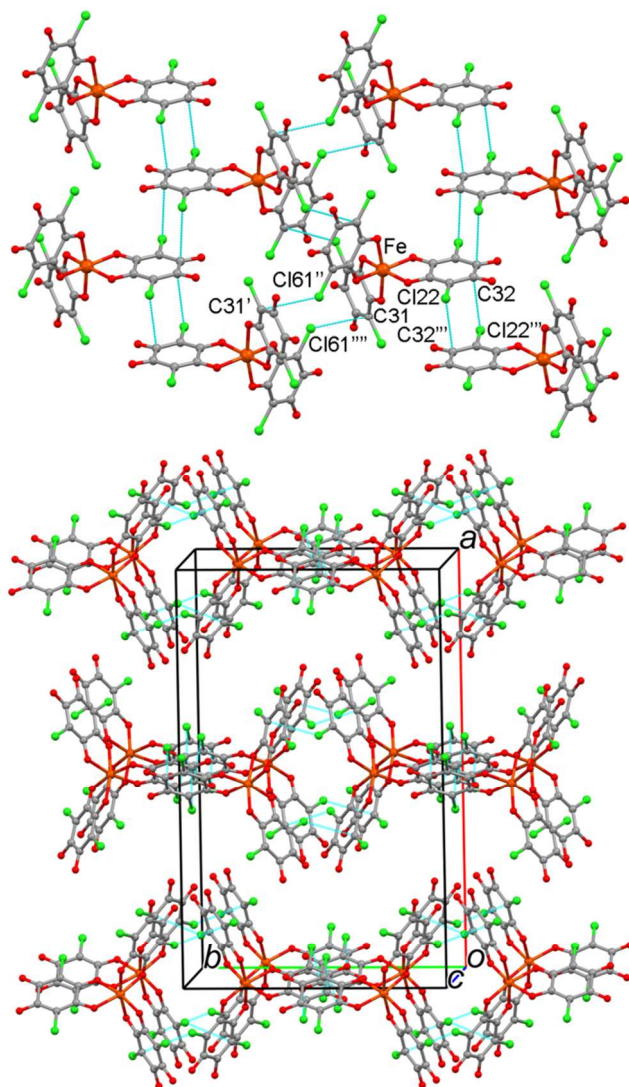


Figure 2 Portion of the molecular packing of **2c** showing the two types of interactions occurring between the complex anions. $(\text{Et})_3\text{NH}^+$ cations and crystallization water molecules were omitted for clarity. Symmetry codes ' = -x; -y; -z, '' = -x; y; $\frac{1}{2}$ -z, ''' = -x; 1-y; -z, '''' = x; -y; z-1/2.

In particular, the ligand comprising the Cl(22) atom is involved in a partial stack with symmetry related ligands and with the shortest distance occurring between Cl(22) and C(32) atoms (3.325(3) Å). At variance, the ligand with Cl(61) interacts with the C(31) atom of an adjacent complex molecule (3.448(4) Å). These interactions determine the formation of irregular layers that are parallel to the *bc* crystallographic plane and that are separated by layers of $(\text{Et})_3\text{NH}^+$ cations. Despite the fact the **1c** complex crystallizes in the monoclinic $P2_1/n$ space group, its crystal packing is very similar to that of **2c** just described. The packing of **5a** shows that the complexes form supramolecular dimers that are held together by two symmetry related I...O

interactions (3.092(8) Å) considerably shorter than the sum of the van der Waals radii of iodine and oxygen (3.50 Å) (Figure 3). The I...O interaction can be regarded as a halogen bond (XB), where the iodine behaves as XB donor and the oxygen atom as the XB acceptor. This is in agreement with the properties of the electrostatic potential for $[\text{Cr}(\text{I}_2\text{An})_3]^{3-}$ that predicts a negative charge accumulation on the peripheral oxygen atoms and a positive charge accumulation on iodine (see below). Given the charge distribution on the halogen atoms, which is mainly located on the portion of the iodine surface opposite to the $\text{C}_{\text{anilate}}\text{-I}$ bond, this interaction is expected to be linear. In fact, the $\text{C}_{\text{anilate}}\text{-I(61)}\cdots\text{O(53)'}$ is 165°. The dinuclear entity held together by two XB is then extensively enveloped by $(n\text{-Bu}_4)\text{N}^+$ cations. Remarkably these XB interactions may be responsible for the weak antiferromagnetic interactions among paramagnetic centers at low temperature observed for this compound (see below), in agreement with the formation of supramolecular dimers.

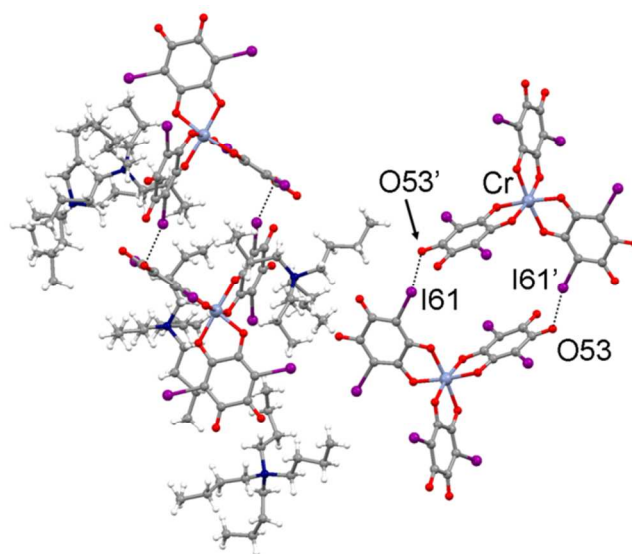


Figure 3 Portion of the molecular packing of **5a**. Four complex anions are displayed. Symmetry code ' = 1-x; 1-y; 1-z.

The **2b** and **4b** complexes are isostructural and therefore their crystal packing can be described together. Moreover, PXRD measurements performed on microcrystalline samples of **1b** and **3b** (Cr(III) complexes) show that these compounds are isostructural to their Fe(III) analogues (**2b**, **4b**) (Figures S8-S9). In these structures, the presence of the $(\text{Ph})_4\text{P}^+$ cations opens the possibility to form π - π interactions between the aromatic rings of the cations and the hexaatomic ring of the three ligands. In fact, the complex anions are embedded in a pocket formed by several $(\text{Ph})_4\text{P}^+$ cations, and each ligand exchanges π - π interactions with a phenyl ring and there is no evidence of a close contact between the complex anions (Figure 4).

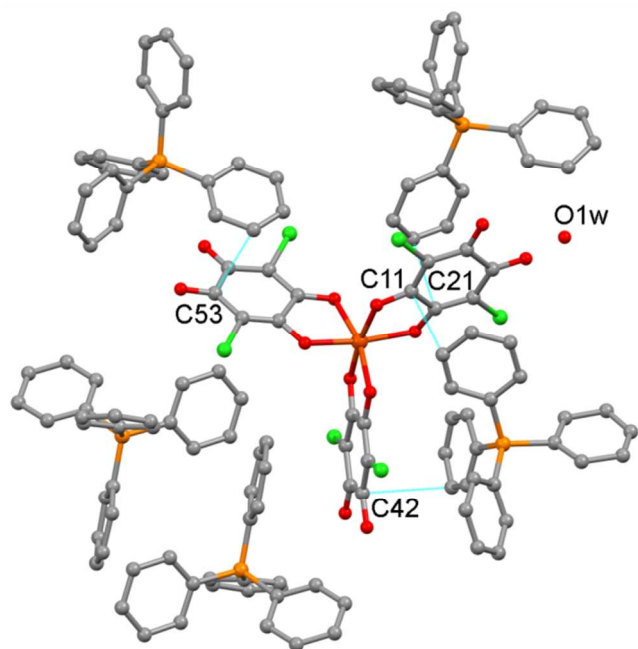


Figure 4 Portion of the molecular packing of **2b** showing the interactions occurring between the complex anion and the surrounding $(\text{Ph})_4\text{P}^+$ cations. Hydrogen atoms were omitted for clarity.

The crystal packing of **6b** shows a series of interactions involving the iodine atoms, the oxygen atoms and the phenyl rings of the $(\text{Ph})_4\text{P}^+$ cation (Figure 5). PXRD measurements performed on a microcrystalline sample of **5b** (Cr(III) complex) show that this compound is isostructural to its Fe(III) analogue (**6b**) (Figures S10). In particular, each $[\text{Fe}(\text{I}_2\text{An})_3]^{3-}$ molecule exchanges three $\text{I}\cdots\text{I}$ XBs with the surrounding complex anions. According to the geometry of the $\text{C}_{\text{anilate}}\text{-I}\cdots\text{I}$ interaction, in the $\text{I}(62)\cdots\text{I}(61)'''$ contact ($3.882(2)$ Å), the $\text{I}(62)$ atom behaves as a XB donor and the $\text{I}(61)'''$ as a XB acceptor ($\text{I}(62)$ is the Lewis acid and $\text{I}(61)'''$ is the base), and with a geometry that is almost linear (162°). The opposite situation is present for the $\text{I}(62)'$ and $\text{I}(61)$ couple. These iodine-iodine interactions form molecular chains parallel to the b axis that are arranged in a molecular layer by means of an additional $\text{I}\cdots\text{I}$ interaction with symmetry related $\text{I}(33)$ atoms ($3.886(2)$ Å). This latter interaction is less directional than the previously described ones, and it appears that each $\text{I}(33)$ atom may behave at the same time as a XB donor and acceptor. Additional XB interaction can be observed by the inspection of the crystal packing of **6b**. In particular, $\text{I}(31)$ interacts with $\text{C}(216)$ ($3.589(1)$ Å) and $\text{I}(61)$ interacts with $\text{C}(205)'''$ ($3.493(1)$ Å). Interestingly, $\text{I}(61)$ behaves as a XB acceptor (Lewis base) with respect to a symmetry related $\text{I}(62)$ and as XB donor (Lewis acid) with respect to $\text{C}(205)'''$. Within each unit cell four pockets surrounded by oxygen atoms of the iodanilate ligands host several crystallization water molecules (Figure 5).

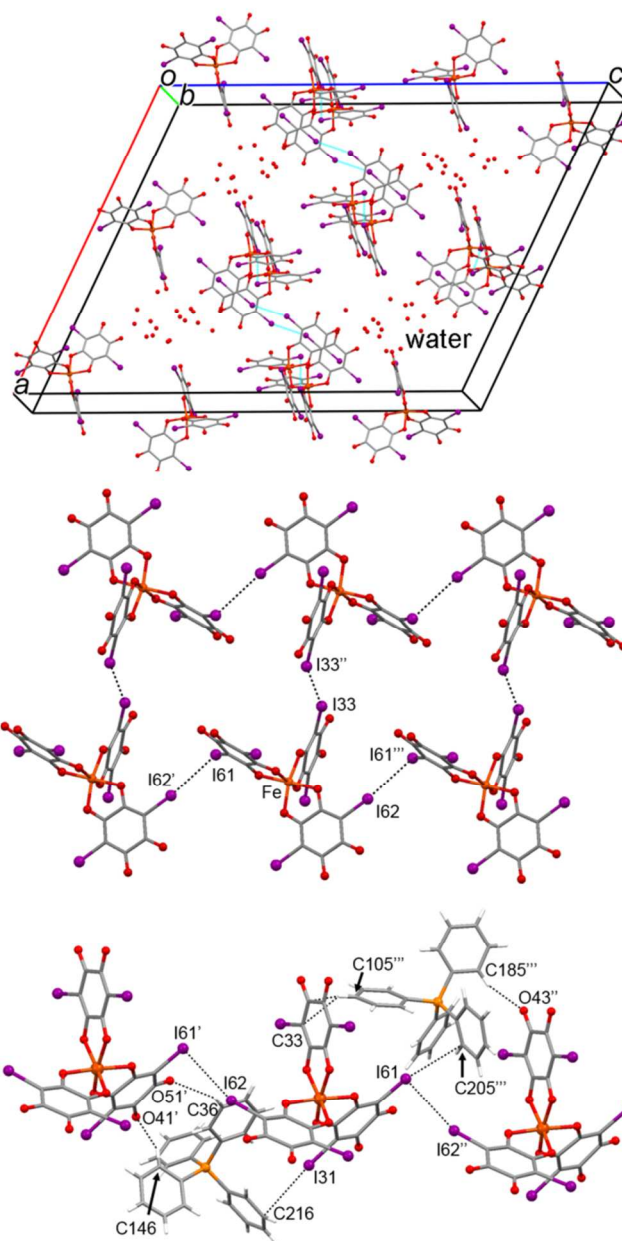


Figure 5 Top, portion of the molecular packing of **6b**. $(\text{Ph})_4\text{P}^+$ cations were omitted for clarity. Middle, halogen bonds between the complex anions. Symmetry codes ' = $x; y+1; z$, '' = $3/2-x; 3/2-y; 1-z$, ''' = $x; y-1; z$. Below, interactions occurring between the complex anions and the surrounding $(\text{Ph})_4\text{P}^+$ cations. Symmetry codes ' = $x; y-1; z$, '' = $x; y+1; z$, ''' = $3/2-x; 5/2-y; 1-z$.

DFT calculations

DFT calculations were performed to gain insight into the electronic structures of the $[\text{M}(\text{X}_2\text{An})_3]^{3-}$ ($\text{M} = \text{Fe}(\text{III}), \text{Cr}(\text{III}); \text{X} = \text{Cl}, \text{Br}, \text{I}$) complexes as well as to characterize the spin and charge distribution of the metal centers and of the three ligands $\text{Cl}_2\text{An}^{2-}$, $\text{Br}_2\text{An}^{2-}$, and I_2An^{2-} . According to the presence of six oxygen atoms in the coordination sphere of the metals and in agreement with magnetic data (see below), the calculations were performed in the high spin states for all of the systems. Two different computational schemes were employed in order

to represent the atomic charges in the six anionic complexes, namely Mulliken and NPA, so as to provide a more complete description of the charge distribution on the different structural fragments.¹¹ By inspecting the Mulliken and NPA charges of the three isolated ligands, it is evident that the negative charge is localized on the four oxygen atoms, whereas there is a slight negative charge accumulation on the halogen atoms, that decreases in the following order Cl > Br > I (Figure 6).

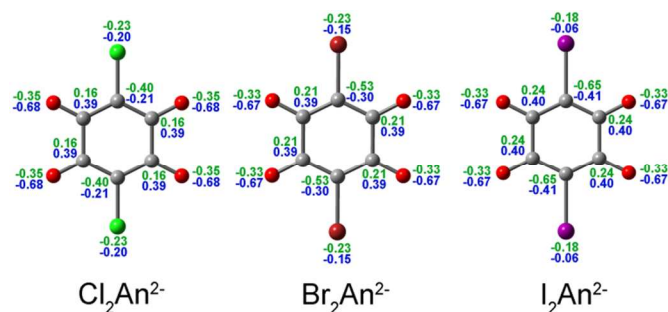


Figure 6 Mulliken (green) and NPA (blue) charges for $\text{Cl}_2\text{An}^{2-}$, $\text{Br}_2\text{An}^{2-}$ and I_2An^{2-} . (B3LYP/SDD with SDD pseudopotentials on Br and I atoms).

According to the NPA charges, when the ligands are coordinated to the metal centers, there is a slight negative charge depletion on the two oxygen atoms that are bound to the metal and also a negative charge depletion on the two peripheral oxygen atoms, which however retain a considerable negative charge (-0.6) (Figures 7).

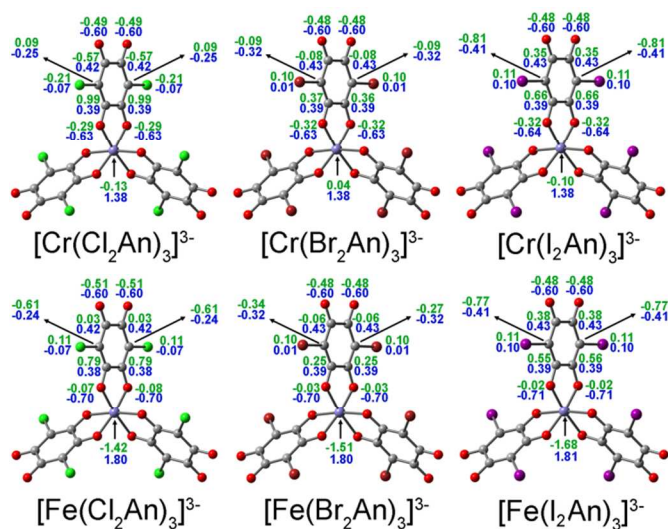


Figure 7 Mulliken (green) and NPA (blue) charges for $[\text{Cr}(\text{Cl}_2\text{An})_3]^{3-}$, $[\text{Cr}(\text{Br}_2\text{An})_3]^{3-}$, $[\text{Cr}(\text{I}_2\text{An})_3]^{3-}$, $[\text{Fe}(\text{Cl}_2\text{An})_3]^{3-}$, $[\text{Fe}(\text{Br}_2\text{An})_3]^{3-}$ and $[\text{Fe}(\text{I}_2\text{An})_3]^{3-}$. (B3LYP/6-31+G(d)-lanl2dz). The charges of only one ligand are depicted for clarity.

On the other hand, the Mulliken analysis predicts that there is a certain degree of negative charge accumulation on the peripheral oxygen atoms. In addition, as observed in the free ligands, the negative charge on the halogen atoms tends to vary in the following order Cl > Br > I, becoming slightly positive in the case of bromine and iodine, either with Mulliken or NPA

schemes. This scenario is identical for both the iron and chromium complexes. A better view of the charge distribution can be obtained by visualizing the electrostatic potential of the complex molecules.^{11,12} In Figure 8 are depicted the isodensity surfaces mapped with the electrostatic potential, and it can be appreciated that the oxygen atoms are regions where there is a marked negative charge accumulation, whereas the metal are the main source of the positive charge. The carbon atoms attached directly to the halogen atoms present a slightly more negative charge than the remaining four carbon atoms of the hexatomic ring. As predicted by the Mulliken or NPA charges, on-going from the $\text{Cl}_2\text{An}^{2-}$ to the I_2An^{2-} ligands there is a positive charge accumulation on the halogen atoms. According to these calculations, it appears that the iodine atoms of I_2An^{2-} in the chromium or iron complexes can behave as XB donors (Lewis acids) whereas the peripheral oxygen atoms can act as XB acceptor (Lewis bases). The weak interactions found in the previously described structures of **5a** and **6b** are in agreement with this description.

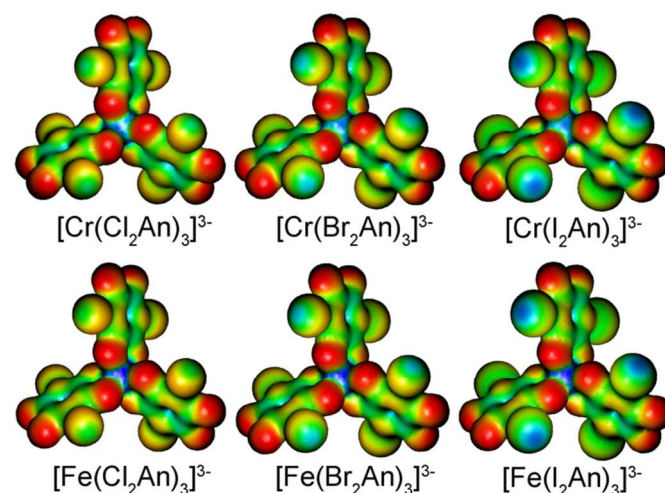


Figure 8 Electrostatic potential for $[\text{Cr}(\text{Cl}_2\text{An})_3]^{3-}$, $[\text{Cr}(\text{Br}_2\text{An})_3]^{3-}$, $[\text{Cr}(\text{I}_2\text{An})_3]^{3-}$, $[\text{Fe}(\text{Cl}_2\text{An})_3]^{3-}$, $[\text{Fe}(\text{Br}_2\text{An})_3]^{3-}$ and $[\text{Fe}(\text{I}_2\text{An})_3]^{3-}$. (B3LYP/6-31+G(d)-lanl2dz). Color codes thresholds: red -0.3, yellow -0.2, green -0.15, light blue -0.1, blue 0.0.

The spin distribution on the metals for the chromium and iron complexes is approximately 3.1 and 4.2, respectively, pointing to a localized nature of the spin on the chromium centers, and to a less localized spin distribution in the iron complexes, Table 2.

Table 2 Mulliken spin densities of the metal, Mulliken and NPA charges of the metal, and expectation values of the $\langle S^2 \rangle$ operator for the six anionic complexes.

	Mulliken atomic spin densities	Mulliken atomic charges	NPA charges	$\langle S^2 \rangle^a$
$[\text{Fe}(\text{Cl}_2\text{An})]^{3-}$	4.158	-1.421	1.798	8.75
$[\text{Fe}(\text{Br}_2\text{An})]^{3-}$	4.159	-1.507	1.800	8.75
$[\text{Fe}(\text{I}_2\text{An})]^{3-}$	4.167	-1.677	1.805	8.75
$[\text{Cr}(\text{Cl}_2\text{An})]^{3-}$	3.098	-0.125	1.379	3.75
$[\text{Cr}(\text{Br}_2\text{An})]^{3-}$	3.071	0.037	1.380	3.75
$[\text{Cr}(\text{I}_2\text{An})]^{3-}$	3.078	-0.098	1.383	3.75

a) after annihilation of the first spin contaminant.

This is also evidenced by inspecting the shape of total spin density that, for the iron complexes, is markedly distributed over the six oxygen atoms of the coordination sphere. On the other hand, the cubic shape of the total spin density of the chromium complexes reflects the octahedral t_{2g}^3 configuration (Figure 9).¹³

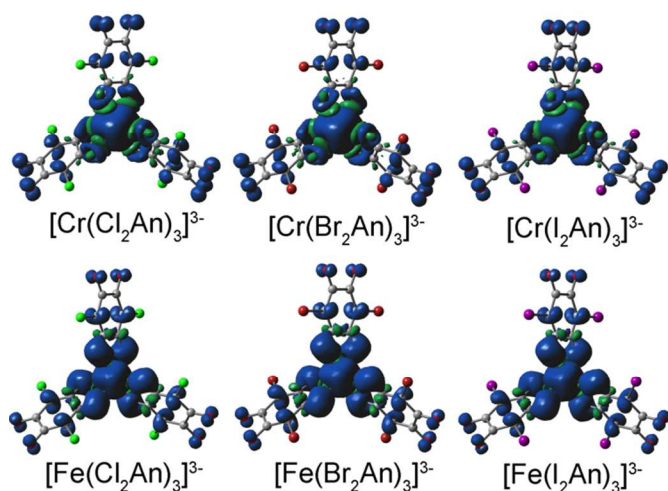


Figure 9 Spin density for $[\text{Cr}(\text{Cl}_2\text{An})_3]^{3-}$, $[\text{Cr}(\text{Br}_2\text{An})_3]^{3-}$, $[\text{Cr}(\text{I}_2\text{An})_3]^{3-}$, $[\text{Fe}(\text{Cl}_2\text{An})_3]^{3-}$, $[\text{Fe}(\text{Br}_2\text{An})_3]^{3-}$ and $[\text{Fe}(\text{I}_2\text{An})_3]^{3-}$ (B3LYP/6-31+G(d)-lanl2dz). Colors blue and green refers to α - and β -spin density, respectively (isosurface plot at 0.0008 esu \AA^{-3}).

Spectroscopic Characterization

As shown in Table 4 and as reported in the Molecular Structure section, compounds **1-6** can crystallize in different space groups, even if they have the same counterion (see for example compounds **1c** and **2c**, and **1b**, **3b** respect to **5b**), hampering an evaluation of their molecular isostructurality using X-ray powder diffraction. To overcome this drawback we performed a detailed spectroscopical study using FT-IR vibrational spectroscopy in order to demonstrate that all the components of this family are isostructural from the molecular point of view (as further confirmation of the obtained analytical data). For shortness we discuss here the FT-IR spectra of compounds **1a-6a** since the FT-IR spectra of compounds **1b-6b** or **1c-2c** show the same features except for the counterion contribution.

VIBRATIONAL SPECTROSCOPY. The infrared spectra of **1a** and **2a** show, in the 3000-2800 cm^{-1} region, the typical $\nu(\text{C-H})$

vibrational modes of the $(n\text{-Bu})_4\text{N}^+$ counterion. A comparison between the spectra of **1a** and **2a** in the 1800-650 cm^{-1} region (Figure S3), showing the same vibrational bands, with similar shape and relative intensity, suggests the same coordination geometry and the same chemical environment for Cr(III) and Fe(III) complexes. According to Pawlukojć *et al.*,¹⁴ the band centered at ca. 1650 cm^{-1} is assigned to the $\nu(\text{C=O})$ vibration mode for the uncoordinated C=O groups of the ligands; a downshift of this band (1665 cm^{-1}) respect to free ligand is observed and it can be attributed to a weakened double bond character of these terminal groups because of the coordination with the metal ion. The strong and broad band centered at ca. 1530 cm^{-1} can be assigned to a $\nu(\text{C=C}) + \nu(\text{C=O})$ combination band; the significant downshift observed (1631 cm^{-1} for the free ligand¹⁴) could be related, also in this case, to the coordination effect. The two bands present in the 1400-1250 cm^{-1} region are assigned to the $\nu(\text{C-C}) + \nu(\text{C-O})$ combination band and $\nu(\text{C-C})$ vibration, respectively, whereas the two ones centered at ca. 995 cm^{-1} e 840 cm^{-1} for both spectra can be related to the $\nu(\text{C-C}) + \nu(\text{C-O}) + \delta(\text{C-Cl})$, and to the $\delta(\text{C=O}) + \delta(\text{C-O}) + \nu(\text{C-Cl})$, combination bands.¹⁴

It is noteworthy that in the 650-400 cm^{-1} region the spectra of the two metal complexes show some differences. Except for the wagging vibrational mode related to the C-Cl bond centered at ca. 570 cm^{-1} for both compounds, three bands at ca. 596, 581 and 505 cm^{-1} are present for **2a** and four bands at ca. 612, 597, 508, 447 cm^{-1} are observed for **1a** (Figure S4). These bands, which are not present in the ligand and counterion spectra, can be related to vibrational modes involving M-O bonds.

Vibrational spectra of compounds **3-6** show similar features in the whole MIR region (4000-400 cm^{-1}) and a summary of the most significative bands with the corresponding assignments is reported in Table S1.

MIR spectra of **2a**, **4a**, and **6a** show similar features with a downward shift of the halogen-sensitive bands as the halogen mass increases, as shown in Figure 10.

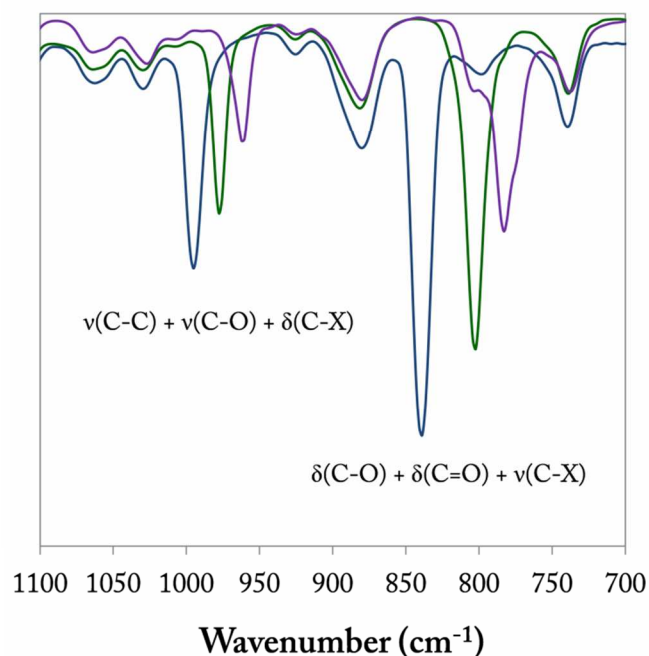


Figure 10 FT-IR spectra (1800–400 cm^{-1}) for **2a** (blue line), **4a** (green line), **6a** (violet line).

These spectroscopic findings confirm that the haloanilate ligands exhibit, in all compounds, the same coordination mode.

Cyclic Voltammetry

Compounds **1-6** were studied by cyclic voltammetry in order to verify their stability toward electrochemical oxidation. Cyclic voltammograms for **1a** and **2a** are reported, as examples, in Figure 11.

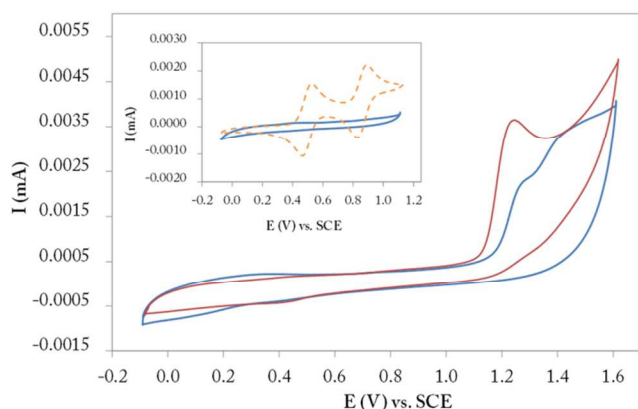


Figure 11 Cyclic voltammograms (-0.1 - 1.6 V) for **1a** (red line) and **2a** (blue line). Inset: cyclic voltammogram (-0.1 - 1.1 V) for **2a** (blue line) superposed with the cyclic voltammogram for BEDT-TTF (orange dashed line) for comparison.

1a shows one irreversible oxidation peak at ca. 1.23 V and **2a** shows two irreversible oxidation peaks at ca. 1.23 and 1.37 V. The same features are observed for all the Cr(III) and Fe(III) compounds (their oxidation potentials are summarized in Table

S2). It is noteworthy that in the 0.0–1.1 V range no oxidation peaks are observed for all compounds. This suggests that these complexes are suitable candidates as counterions toward organic donors such as BEDT-TTF, which shows a mono-electronic reversible oxidation process at ca. 0.5 V (Inset in Figure 11).

Magnetic Properties

The thermal variation of the molar magnetic susceptibility per Fe(III) ion expressed as $\chi_m T$ for compounds **2b**, **4b**, and **6b** is shown in Figure 12. These compounds show similar behaviors with $\chi_m T$ values at room temperature of ca. $4.4 \text{ cm}^3 \text{ mol}^{-1} \text{ K}$, close to the expected value ($4.375 \text{ cm}^3 \text{ mol}^{-1} \text{ K}$) for isolated high spin Fe(III) ions ($S = 5/2$, $g = 2$). These values remain constant down to ca. 15 K, then the $\chi_m T$ product decreases. The observed behavior in the high temperature region is typical of magnetically isolated $S = 5/2$ ions. The observed decrease at low temperature may be due to weak antiferromagnetic interactions between the Fe(III) ions and/or to the presence of a zero-field splitting (ZFS) in the $S = 5/2$ ground state of the Fe(III) complexes. Taking into account the crystallographic data for **2b**, **4b**, and **6b**, which indicate either slightly-distorted octahedral coordination geometries around the Fe(III) ions (see above) or Fe(III) ions quite isolated in the crystal structure (in particular for **2b** and **4b**), it seems reasonable to use a model that considers isolated $S = 5/2$ ions with a ZFS parameter (D) to fit the $\chi_m T$ vs. T magnetic data.¹⁵

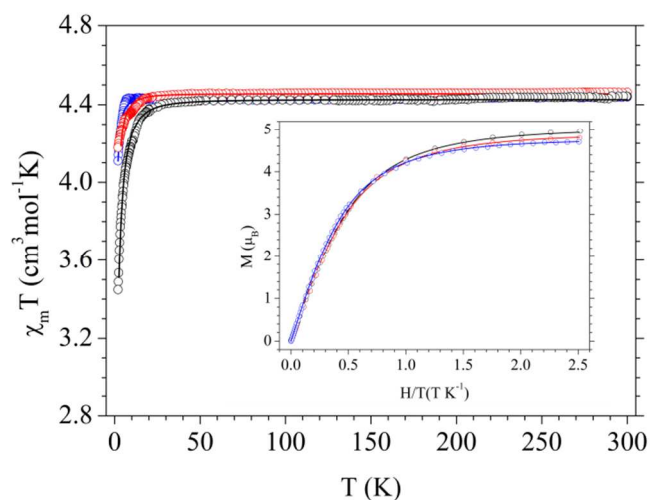


Figure 12 Thermal variation of the $\chi_m T$ product for **2b** (black circles), **4b** (red circles), and **6b** (blue circles). Solid lines are the best fit of the model (see text). Inset shows the isothermal magnetization at 2 K for **2b**, **4b**, and **6b** (same colour codes).

This model satisfactorily reproduces the magnetic properties of compounds **2b**, **4b**, and **6b** in the whole temperature range, with $g = 1.987(1)$, $2.006(1)$, $2.017(1)$, and $|D| = 2.3(1)$, $0.62(1)$, $0.94(1) \text{ cm}^{-1}$, for **2b**, **4b**, and **6b** respectively. Unfortunately, since magnetic measurements were performed on microcrystalline samples, we were not able to determine the sign of D . The isothermal magnetization measurements (Inset in Figure 12) support the $S = 5/2$ ground spin state of the Fe(III)

ions for all **2b**, **4b**, and **6b**, since they can be well reproduced with a Brillouin function for a $S = 5/2$ spin state. Thus, compounds **2b**, **4b**, and **6b**, present a high spin configuration for the Fe(III) ions with a $S = 5/2$ ground spin state and show a typical paramagnetic behaviour of isolated ions. All Fe(III) compounds described in this work show analog magnetic behavior and a comparison of the thermal variation of $\chi_m T$ for **2a**, **2b**, and **2c**, (same anionic complex with different counterions) is reported in Figure S14.

The thermal variation of the molar magnetic susceptibility per Cr(III) ion expressed as $\chi_m T$ for compounds **1b**, **3b**, and **5b** is shown in Figure 13. These compounds show similar behaviors with $\chi_m T$ values a room temperature of ca. 1.9 $\text{cm}^3\text{mol}^{-1}\text{K}$, close to the expected value (1.875 $\text{cm}^3\text{mol}^{-1}\text{K}$) for isolated Cr(III) ions ($S = 3/2$, $g = 2$). These values remain constant down to ca. 10 K, then the $\chi_m T$ product decreases. The observed behavior in the high temperature region is typical of magnetically isolated $S = 3/2$ ions. As in the Fe(III) complexes, the observed decrease at low temperature may be due to weak antiferromagnetic interactions between the Cr(III) ions and/or to the presence of a ZFS in the $S = 3/2$ ground state of the Cr(III) complexes. Taking into account the same structural considerations, since $(\text{Ph})_4\text{P}^+$ salts of Cr(III) and Fe(III) complexes are isostructural, it seems reasonable to use a model that consider isolated $S = 3/2$ ions with a ZFS parameter (D) to fit the $\chi_m T$ vs. T magnetic data.¹⁵

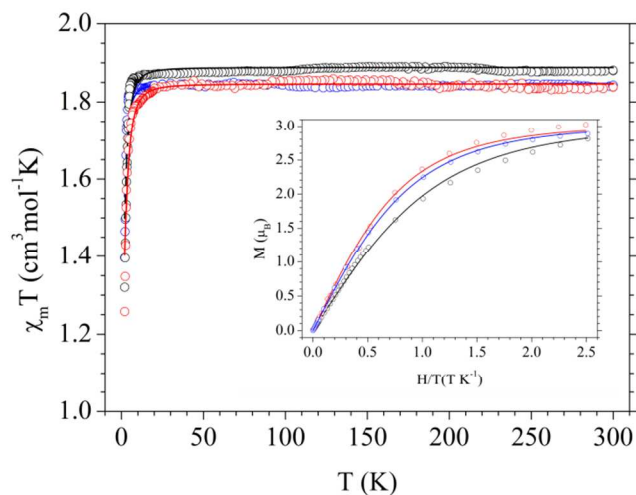


Figure 13 Thermal variation of the $\chi_m T$ product for **1b** (black circles), **3b** (red circles), and **5b** (blue circles). Solid lines are the best fit of the model (see text). Inset shows the isothermal magnetization at 2 K for **1b**, **3b**, and **5b** (same colour codes).

This model satisfactorily reproduces the magnetic properties of compounds **1b**, **3b**, and **5b** in the whole temperature range, with $g = 1.994(1)$, $1.992(1)$, $2.024(1)$, and $|D| = 4.2(1)$, $4.0(1)$, $3.0(1)$ cm^{-1} , for **1b**, **3b**, and **5b** respectively. The isothermal magnetization measurements (Inset in Figure 13) support the $S = 3/2$ ground spin state of the Cr(III) ions for all **1b**, **3b**, and **5b**, since they can be well reproduced with a Brillouin function for a $S = 3/2$ spin state. Thus, compounds **2b**, **4b**, and **6b**, present

Cr(III) ions with a $S = 3/2$ ground spin state and show a typical paramagnetic behaviour of isolated ions.

Interestingly, compound **5a** presents a unique magnetic behavior among these complexes. For this Cr(III) complex, the thermal trend of the $\chi_m T$ product decreases much more than in the others, i.e. decreases from the room temperature expected value of about 1.88 $\text{cm}^3\text{mol}^{-1}\text{K}$ down to 0.5 $\text{cm}^3\text{mol}^{-1}\text{K}$ at 2 K (Figure S15); this is due to the unique trend of the molar magnetic susceptibility χ_m , which reaches a maximum at 4.1(1) K and decreases down to 2 K (Figure 14). Moreover, the isothermal magnetization measurements performed on **5a** (Inset in Figure 14) do not show the typical behavior of isolated $S = 3/2$ ions, because it appears quite linear and does not reach the expected saturation value of $3\mu_B$.

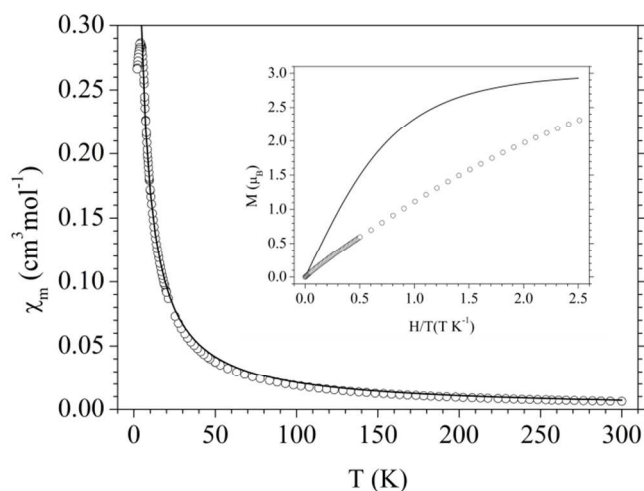


Figure 14 Thermal variation of χ_m for **5a**. Solid line is the best fit to the Curie-Weiss law (see text). Inset shows the isothermal magnetization at 2 K for **5a**. Solid line represents the Brillouin function for an isolated $S = 3/2$ ion with $g = 2$.

The observed behaviour at low temperature is likely due to magnetic interactions between the Cr(III) ions. This behaviour can be explained considering the crystallographic data for this compound. As described in the Molecular Structure Section, **5a** is formed by supramolecular dimers that are held together by two symmetry related I...O interactions (3.092(8) Å) (Figure 3) considerably shorter than the sum of iodine and oxygen van der Waals radii (3.50 Å). These halogen-bonding interactions may be responsible for an additional antiferromagnetic coupling between different anionic complexes associated in dimers, due to the extended iodine orbitals which can mediate exchange interactions, as already observed in the literature.¹⁶ In this case, the simple model that consider isolated $S = 3/2$ ions only with a ZFS parameter does not fit the magnetic data satisfactorily, suggesting that a better fit can be obtained by taking into account magnetic interactions between ions. For this reason, the susceptibility was fitted using the Curie-Weiss law

$$\chi_m(T) = Np^2\mu_B^2/[3k(T-\theta)] \quad (1)$$

where N is the number of magnetic ions in a mole, $p = g[S(S+1)]^{1/2}$ is the effective number of Bohr magnetons, μ_B is the Bohr magneton, k is the Boltzmann constant and θ is the Weiss constant.¹⁵ The fit has been performed in the paramagnetic region, where this law holds, i.e. above the temperature of the maximum; the fit gives an effective Bohr magneton number $p = 4.2(1)$ and a Weiss constant $\theta = -2.8(1)$ K. The negative Weiss constant points out that the interactions between Cr(III) ions are antiferromagnetic; this is confirmed by the low isothermal magnetization and by the maximum of χ_m at 4.1(1) K, which identifies the transition to the magnetically ordered antiferromagnetic state.¹⁵

The other Cr(III) compounds described in these work show a typical paramagnetic behavior, and a comparison of the thermal variation of $\chi_m T$ for **1a**, **1b**, and **1c**, (same anionic complex with different counterions) is reported in Figure S16.

Experimental

General Remarks

Bromanilic acid (hereafter H₂Br₂An) and Iodanilic acid (hereafter H₂I₂An) were synthesized according to literature methods.¹⁷ All the others chemicals used in the synthesis were purchased and used without further purification.

Synthesis

[(*n*-Bu)₄N]₃[Cr(Cl₂An)₃] (1a). An aqueous solution (5 mL) of CrCl₃·6H₂O (210 mg, 0.80 mmol) was added dropwise to an aqueous solution (50 mL) of H₂Cl₂An (500 mg, 2.4 mmol), NaOH (200 mg, 5.0 mmol) and (*n*-Bu)₄NBr (800 mg, 2.5 mmol). After ca. 30 min at 60 °C, **1a** starts to precipitate as red-violet solid, partially soluble in water. The mixture was allowed to cool to 25 °C, extracted with CH₂Cl₂ and dried under Na₂SO₄. The solution was filtered, rota-evaporated, and the obtained lacquer-like solid was crystallized in a MeOH/CH₂Cl₂ mixture to give red shiny crystals. Yield: 73%. Elemental anal. Calcd for C₆₆H₁₀₈Cl₆CrN₃O₁₂: C, 56.61; H, 7.77; N, 3.00; Found. C, 56.38; H, 7.71; N, 2.83. FT-IR ($\nu_{\max}/\text{cm}^{-1}$, KBr pellets): 2962(m), 2933(w), 2875(m), 1649(m), 1531(vs), 1469(w), 1383(w), 1353(s), 1303(m), 1000(m), 880(w), 841(m), 739(vw), 612(m), 597(w), 572(w), 508(w), 447(w). UV-Vis (CH₃CN solution, λ_{\max}/nm ($\epsilon/\text{dm}^3 \text{ mol}^{-1} \text{ cm}^{-1}$)): 466 sh, 497 (4493), 570 sh. ESI-MS, m/z Found (Calcd) = 1156.27 (1154.26) $[[(\textit{n}\text{-Bu})_4\text{N}]_2[\text{Cr}(\text{Cl}_2\text{An})_3]]^+$; 914.99 (915.00) $[[(\textit{n}\text{-Bu})_4\text{N}][\text{Cr}(\text{Cl}_2\text{An})_3]\text{-H}]^+$; 456.99 (455.99) $[[(\textit{n}\text{-Bu})_4\text{N}][\text{Cr}(\text{Cl}_2\text{An})_3]]^{2-}$.

[(Ph)₄P]₃[Cr(Cl₂An)₃]·H₂O (1b). An aqueous solution (5 mL) of CrCl₃·6H₂O (210 mg, 0.80 mmol) was added dropwise to an aqueous solution (50 mL) of H₂Cl₂An (500 mg, 2.4 mmol), NaOH (200 mg, 5.0 mmol) and (Ph)₄PBr (1050 mg, 2.5 mmol). **1b** precipitates as red-violet solid. The mixture was allowed to cool to 25 °C, and then the precipitate was collected by filtration, washed several times with fresh water and dried in desiccator. Yield: 80%. The product was recrystallized from a

MeOH/CH₂Cl₂ mixture. Elemental anal. Calcd for C₉₀H₆₂Cl₆CrP₃O₁₃: C, 63.25; H, 3.66; Found. C, 62.88; H, 3.61. FT-IR ($\nu_{\max}/\text{cm}^{-1}$, KBr pellets): 3059(m), 3023(w), 2993(w), 1646(m), 1587(w), 1531(vs), 1438(s), 1352(vs), 1305(m), 1189(w), 1165(w), 1108(s), 1000(m), 843(m), 816(w), 756(m), 724(s), 690(m), 611(m), 571(w), 528(s), 449(w). UV-Vis (CH₃CN solution, λ_{\max}/nm ($\epsilon/\text{dm}^3 \text{ mol}^{-1} \text{ cm}^{-1}$)): 466 sh, 497 (3878), 570 sh. ESI-MS, m/z Found (Calcd) = 1349.67 (1351.68) $[[(\text{Ph})_4\text{P}]_2[\text{Cr}(\text{Cl}_2\text{An})_3]]^+$; 1013.48 (1013.49) $[[(\text{Ph})_4\text{P}][\text{Cr}(\text{Cl}_2\text{An})_3]\text{-H}]^+$; 506.15 (505.03) $[[(\text{Ph})_4\text{P}][\text{Cr}(\text{Cl}_2\text{An})_3]]^{2-}$.

[(Et)₃NH]₃[Cr(Cl₂An)₃]·H₂O (1c). Triethylamine (0.7 mL, 9.5 mmol) was added to a CH₃CN solution (50 mL) of H₂Cl₂An (500 mg, 2.4 mmol), then an aqueous solution (15 mL) of KCr(SO₄)₂·12H₂O (400 mg, 0.80 mmol) was added dropwise to the CH₃CN solution. The resulting mixture was heated up to reflux for 12 hours. **1c** precipitates as red shiny crystals suitable for X-ray analysis after slow evaporation of the mother liquor. Yield: 78%. Elemental anal. Calcd for C₃₆H₅₀Cl₆CrN₃O₁₃: C, 43.35; H, 5.05; N, 4.21; Found. C, 42.89; H, 4.93; N, 4.15. FT-IR ($\nu_{\max}/\text{cm}^{-1}$, KBr pellet): 3567(m), 3497(m), 3036(m), 2985(w), 2862(w), 1653(m), 1630(s), 1530(vs), 1472(s), 1357(vs), 1325(s), 1264(w), 1159(w), 1059(w), 1003(m), 846(s), 616(s), 573(m), 512(m), 450(m), 404(w). UV-Vis (CH₃CN solution, λ_{\max}/nm ($\epsilon/\text{dm}^3 \text{ mol}^{-1} \text{ cm}^{-1}$)): 466 sh, 497 (4235), 570 sh. ESI-MS, m/z Found (Calcd) = 1080.10 (1080.18) $[[(\text{Et})_3\text{NH}]_4[\text{Cr}(\text{Cl}_2\text{An})_3]]^+$; 978.56 (979.36) $[[(\text{Et})_3\text{NH}]_3[\text{Cr}(\text{Cl}_2\text{An})_3]\text{-H}]^+$; 878.56 (878.64) $[[(\text{Et})_3\text{NH}]_2[\text{Cr}(\text{Cl}_2\text{An})_3]\text{-2H}]^+$.

[(*n*-Bu)₄N]₃[Fe(Cl₂An)₃] (2a). This compound was synthesized as dark-violet shiny crystals according to the procedure described for **1a**, using FeCl₃ (130 mg, 0.80 mmol), H₂Cl₂An (500 mg, 2.4 mmol), NaOH (200 mg, 5.0 mmol) and (*n*-Bu)₄NBr (800 mg, 2.5 mmol). Yield: 80%. Elemental anal. Calcd for C₆₆H₁₀₈Cl₆FeN₃O₁₂: C, 56.46; H, 7.75; N, 2.99; Found. C, 56.47; H, 7.83; N, 3.03. FT-IR ($\nu_{\max}/\text{cm}^{-1}$, KBr pellets): 2962(m), 2933(w), 2875(m), 1647(m), 1531(vs), 1469(w), 1383(w), 1349(s), 1300(s), 995(m), 878(w), 839(w), 739(w), 596(m), 574(m), 506(m). UV-Vis (CH₃CN solution, λ_{\max}/nm ($\epsilon/\text{dm}^3 \text{ mol}^{-1} \text{ cm}^{-1}$)): 444 (3669), 477 (4494), 516 (4910). ESI-MS, m/z Found (Calcd) = 1160.24 (1158.26) $[[(\textit{n}\text{-Bu})_4\text{N}]_2[\text{Fe}(\text{Cl}_2\text{An})_3]]^+$; 918.94 (918.99) $[[(\textit{n}\text{-Bu})_4\text{N}][\text{Fe}(\text{Cl}_2\text{An})_3]\text{-H}]^+$; 458.98 (457.98) $[[(\textit{n}\text{-Bu})_4\text{N}][\text{Fe}(\text{Cl}_2\text{An})_3]]^{2-}$.

[(Ph)₄P]₃[Fe(Cl₂An)₃]·H₂O (2b). This compound was synthesized as dark-violet shiny crystals according to the procedure described for **1b**, using FeCl₃ (130 mg, 0.80 mmol), H₂CA (500 mg, 2.4 mmol), NaOH (200 mg, 5.0 mmol) and (Ph)₄PBr (1050 mg, 2.5 mmol). Yield: 85%. Elemental anal. Calcd for C₉₀H₆₂Cl₆FeP₃O₁₃: C, 63.11; H, 3.65; Found. C, 62.75; H, 3.31. FT-IR ($\nu_{\max}/\text{cm}^{-1}$, KBr pellets): 3059(m), 3023(w), 2993(w), 1644(m), 1587(w), 1528(vs), 1438(s), 1350(vs), 1304(m), 1188(w), 1165(w), 1108(s), 996(m),

839(m), 755(m), 724(s), 690(m), 597(m), 573(w), 528(s), 507(w). UV-Vis (CH₃CN solution, $\lambda_{\text{max}}/\text{nm}$ ($\epsilon/\text{dm}^3 \text{ mol}^{-1} \text{ cm}^{-1}$)): 444 (3823), 477 (4617), 516 (5075). ESI-MS, m/z Found (Calcd) = 1353.57 (1355.48) $[[(\text{Ph})_4\text{P}]_2[\text{Fe}(\text{Cl}_2\text{An})_3]]^-$; 1016.09 (1015.39) $[[(\text{Ph})_4\text{P}][\text{Fe}(\text{Cl}_2\text{An})_3]\text{-H}]^-$; 507.19 (508.05) $[[(\text{Ph})_4\text{P}][\text{Fe}(\text{Cl}_2\text{An})_3]]^{2-}$.

[(Et)₃NH]₃[Fe(Cl₂An)₃·H₂O (2c). This compound was synthesized as dark-violet crystals according to the procedure described for **1c**, using Fe(ClO₄)₃·6H₂O (290 mg, 0.80 mmol), H₂Cl₂An (0.5 g, 2.4 mmol) and triethylamine (0.7 mL, 9.5 mmol). Yield: 84%. Elemental anal. Calcd for C₃₆H₅₀Cl₆FeN₃O₁₃: C, 43.18; H, 5.03; N, 4.20; Found. C, 42.78; H, 4.83; N, 4.08. FT-IR ($\nu_{\text{max}}/\text{cm}^{-1}$, KBr pellets): 3567(m), 3497(m), 3039(m), 2985(w), 2866(w), 1651(m), 1633(m), 1530(vs), 1472(s), 1359(vs), 1322(s), 1264(w), 1159(w), 1059(w), 996(m), 841(s), 601(s), 575(m), 512(m), 404(w). UV-Vis (CH₃CN solution, $\lambda_{\text{max}}/\text{nm}$ ($\epsilon/\text{dm}^3 \text{ mol}^{-1} \text{ cm}^{-1}$)): 444 (3750), 477 (4523), 516 (5010). ESI-MS, m/z Found (Calcd) = 1083.98 (1084.03) $[[(\text{Et})_3\text{NH}]_4[\text{Fe}(\text{Cl}_2\text{An})_3]]^+$; 982.63 (983.21) $[[(\text{Et})_3\text{NH}]_3[\text{Fe}(\text{Cl}_2\text{An})_3]\text{-H}]^+$; 881.51 (882.39) $[[(\text{Et})_3\text{NH}]_2[\text{Fe}(\text{Cl}_2\text{An})_3]\text{-2H}]^+$.

[(n-Bu)₄N]₃[Cr(Br₂An)₃] (3a). This compound was synthesized as red shiny crystals according to the procedure described for **1a**, using CrCl₃·6H₂O (61 mg, 0.22 mmol), H₂Br₂An (194 mg, 0.65 mmol), NaOH (52 mg, 1.3 mmol) and (n-Bu)₄NBr (213 mg, 0.66 mmol). Yield: 70%. Elemental anal. Calcd for C₆₆H₁₀₈Br₆CrN₃O₁₂: C, 47.55; H, 6.53; N, 2.52; Found. C, 47.22; H, 6.43; N, 2.33. FT-IR ($\nu_{\text{max}}/\text{cm}^{-1}$, KBr pellets): 2962(m), 2933(w), 2873(m), 1638(m), 1620(m), 1521(vs), 1343(s), 1310(m), 989(m), 883(w), 813(m), 736(w), 613(m), 594(w), 559(m), 507(m), 472(vw), 413(w). UV-Vis (CH₃CN solution, $\lambda_{\text{max}}/\text{nm}$ ($\epsilon/\text{dm}^3 \text{ mol}^{-1} \text{ cm}^{-1}$)): 455 (4347), 490 (5115), 555 sh. ESI-MS, m/z Found (Calcd) = 1423.92 (1424.55) $[[(\text{n-Bu})_4\text{N}]_2[\text{Cr}(\text{Br}_2\text{An})_3]]^-$; 1182.66 (1185.10) $[[(\text{n-Bu})_4\text{N}][\text{Cr}(\text{Br}_2\text{An})_3]\text{-H}]^-$.

[(Ph)₄P]₃[Cr(Br₂An)₃·H₂O (3b). This compound was synthesized as red shiny crystals according to the procedure described for **1b**, using CrCl₃·6H₂O (61 mg, 0.22 mmol), H₂Br₂An (194 mg, 0.65 mmol), NaOH (52 mg, 1.3 mmol) and (Ph)₄PBr (277 mg, 0.66 mmol). Yield: 83%. Elemental anal. Calcd for C₉₀H₆₂Br₆CrP₃O₁₃: C, 54.71; H, 3.16; Found. C, 54.32; H, 3.03. FT-IR ($\nu_{\text{max}}/\text{cm}^{-1}$, KBr pellets): 3059(m), 3023(w), 2993(w), 1639(m), 1586(w), 1521(vs), 1438(s), 1364(m), 1341(vs), 1299(m), 1283(m), 1187(w), 1165(w), 1109(s), 1000(m), 986(m), 812(m), 756(m), 724(s), 690(m), 603(m), 558(w), 527(s), 501(m), 459(w). UV-Vis (CH₃CN solution, $\lambda_{\text{max}}/\text{nm}$ ($\epsilon/\text{dm}^3 \text{ mol}^{-1} \text{ cm}^{-1}$)): 455 (3385), 490 (4403), 555 sh. ESI-MS, m/z Found (Calcd) = 1279.14 (1280.00) $[[(\text{Ph})_4\text{P}][\text{Cr}(\text{Br}_2\text{An})_3]\text{-H}]^-$; 641.21 (639.50) $[[(\text{Ph})_4\text{P}][\text{Cr}(\text{Br}_2\text{An})_3]]^{2-}$.

[(n-Bu)₄N]₃[Fe(Br₂An)₃] (4a). This compound was synthesized as violet shiny crystals according to the procedure described for

1a, using FeCl₃ (35 mg, 0.22 mmol), H₂Br₂An (194 mg, 0.65 mmol), NaOH (52 mg, 1.3 mmol) and (n-Bu)₄NBr (213 mg, 0.66 mmol). Yield: 75%. Elemental anal. Calcd for C₆₆H₁₀₈Br₆FeN₃O₁₂: C, 47.44; H, 6.52; N, 2.51; Found. C, 46.98; H, 6.31; N, 2.52. FT-IR ($\nu_{\text{max}}/\text{cm}^{-1}$, KBr pellets): 2962(m), 2933(w), 2875(m), 1640(m), 1620(m), 1521(vs), 1472(m), 1338(s), 1281(m), 978(m), 883(w), 803(m), 739(w), 576(m), 562(m), 500(w). UV-Vis (CH₃CN solution, $\lambda_{\text{max}}/\text{nm}$ ($\epsilon/\text{dm}^3 \text{ mol}^{-1} \text{ cm}^{-1}$)): 443 (5487), 477 (6439), 519 (6841). ESI-MS, m/z Found (Calcd) = 1427.90 (1428.40) $[[(\text{n-Bu})_4\text{N}]_2[\text{Fe}(\text{Br}_2\text{An})_3]]^-$; 1186.59 (1188.95) $[[(\text{n-Bu})_4\text{N}][\text{Fe}(\text{Br}_2\text{An})_3]\text{-H}]^-$.

[(Ph)₄P]₃[Fe(Br₂An)₃·H₂O (4b). This compound was synthesized as dark-violet shiny crystals according to the procedure described for **1b**, using FeCl₃ (35 mg, 0.22 mmol), H₂Br₂An (194 mg, 0.65 mmol), NaOH (52 mg, 1.3 mmol) and (Ph)₄PBr (277 mg, 0.66 mmol). Yield: 83%. Elemental anal. Calcd for C₉₀H₆₂Br₆FeP₃O₁₃: C, 54.60; H, 3.16; Found. C, 54.13; H, 2.98. FT-IR ($\nu_{\text{max}}/\text{cm}^{-1}$, KBr pellets): 3059(m), 3023(w), 2993(w), 1640(m), 1586(w), 1519(vs), 1438(s), 1336(vs), 1281(m), 1188(w), 1164(w), 1109(s), 997(m), 979(m), 804(m), 756(m), 724(s), 690(m), 580(m), 559(w), 530(s), 501(m), 459(w). UV-Vis (CH₃CN solution, $\lambda_{\text{max}}/\text{nm}$ ($\epsilon/\text{dm}^3 \text{ mol}^{-1} \text{ cm}^{-1}$)): 443 (6323), 477 (6856), 519 (6535). ESI-MS, m/z Found (Calcd) = 1621.29 (1622.23) $[[(\text{Ph})_4\text{P}]_2[\text{Fe}(\text{Br}_2\text{An})_3]]^-$; 1283.09 (1283.84) $[[(\text{Ph})_4\text{P}][\text{Fe}(\text{Br}_2\text{An})_3]\text{-H}]^-$; 640.89 (641.42) $[[(\text{Ph})_4\text{P}][\text{Fe}(\text{Br}_2\text{An})_3]]^{2-}$.

[(n-Bu)₄N]₃[Cr(I₂An)₃] (5a). This compound was synthesized as dark-red shiny crystals according to the procedure described for **1a**, using CrCl₃·6H₂O (88 mg, 0.33 mmol), H₂I₂An (392 mg, 1.0 mmol), NaOH (80 mg, 2.0 mmol) and NBu₄Br (387 mg, 1.2 mmol). Yield: 74%. Elemental anal. Calcd for C₆₆H₁₀₈I₆CrN₃O₁₂: C, 40.67; H, 5.59; N, 2.16; Found. C, 40.37; H, 5.59; N, 2.16. FT-IR ($\nu_{\text{max}}/\text{cm}^{-1}$, KBr pellets): 2962(m), 2933(w), 2873(m), 1630(s), 1513(vs), 1330(s), 1270(m), 968(m), 881(w), 791(m), 778(m), 738(w), 698(m), 549(m), 501(m). UV-Vis (CH₃CN solution, $\lambda_{\text{max}}/\text{nm}$ ($\epsilon/\text{dm}^3 \text{ mol}^{-1} \text{ cm}^{-1}$)): 463 sh, 502 (5102), 575 sh. ESI-MS, m/z Found (Calcd) = 1705.90 (1705.87) $[[(\text{n-Bu})_4\text{N}]_2[\text{Cr}(\text{I}_2\text{An})_3]]^-$.

[(Ph)₄P]₃[Cr(I₂An)₃·H₂O (5b). This compound was synthesized as dark-red shiny crystals according to the procedure described for **1b**, using CrCl₃·6H₂O (59 mg, 0.22 mmol), H₂I₂An (255 mg, 0.65 mmol), NaOH (52 mg, 1.3 mmol) and (Ph)₄PBr (277 mg, 0.66 mmol). Yield: 84%. Elemental anal. Calcd for C₉₀H₆₂I₆CrP₃O₁₃: C, 47.88; H, 2.77; Found. C, 47.29; H, 2.63. FT-IR ($\nu_{\text{max}}/\text{cm}^{-1}$, KBr pellets): 3059(m), 3023(w), 2993(w), 1630(m), 1585(w), 1511(vs), 1437(s), 1330(vs), 1274(m), 1188(w), 1164(w), 1108(s), 997(m), 969(m), 790(m), 778(m), 754(m), 723(s), 689(s), 590(m), 548(m), 527(s), 503(m), 456(w). UV-Vis (CH₃CN solution, $\lambda_{\text{max}}/\text{nm}$ ($\epsilon/\text{dm}^3 \text{ mol}^{-1} \text{ cm}^{-1}$)): 463 sh, 502 (5003), 575 sh. ESI-MS, m/z Found (Calcd) = 1562.76 (1562.00)

$[(Ph)_4P][Cr(I_2An)_3]-H]^-$; 779.86 (780.50)
 $[(Ph)_4P][Cr(I_2An)_3]^{2-}$.

[(*n*-Bu)₄N]₃[Fe(I₂An)₃] (6a). This compound was synthesized as dark-violet shiny crystals according to the procedure described for **1a**, using FeCl₃ (54 mg, 0.33 mmol), H₂I₂An (390 mg, 1.0 mmol), NaOH (80 mg, 2.0 mmol) and NBu₄Br (330 mg, 1.0 mmol). Yield: 85%. Elemental anal. Calcd for C₆₆H₁₀₈I₆FeN₃O₁₂: C, 40.59; H, 5.57; N, 2.15; Found. C, 39.15; H, 5.03; N, 2.04. FT-IR (ν_{max}/cm^{-1} , KBr pellets): 2962(m), 2932(w), 2872(m), 1630(s), 1515(vs), 1325(s), 1269(m), 962(m), 878(w), 795(m), 781(m), 736(w), 588(m), 551(m), 497(m). UV-Vis (CH₃CN solution, λ_{max}/nm ($\epsilon/dm^3 mol^{-1} cm^{-1}$)): 450 (6210), 479 (6098), 530 sh. ESI-MS, *m/z* Found (Calcd) = 1709.81 (1709.87) $[(n-Bu)_4N]_2[Fe(I_2An)_3]^-$.

[(Ph)₄P]₃[Fe(I₂An)₃]-4H₂O (6b). This compound was synthesized as dark-violet shiny crystals according to the procedure described for **2b**, using FeCl₃ (35 mg, 0.22 mmol), H₂I₂An (255 mg, 0.65 mmol), NaOH (52 mg, 1.3 mmol) and (Ph)₄PBr (277 mg, 0.66 mmol). Yield: 90%. Elemental anal. Calcd for C₉₀H₆₈I₆FeP₃O₁₆: C, 46.68; H, 2.96; Found. C, 46.42; H, 2.81. FT-IR (ν_{max}/cm^{-1} , KBr pellets): 3059(m), 3023(w), 2993(w), 1629(m), 1585(w), 1515(vs), 1436(s), 1325(vs), 1266(m), 1189(w), 1163(w), 1107(s), 996(m), 962(m), 783(m), 757(m), 723(s), 689(m), 578(m), 550(w), 527(s), 499(m). UV-Vis (CH₃CN solution, λ_{max}/nm ($\epsilon/dm^3 mol^{-1} cm^{-1}$)): 450 (5770), 479 (6088), 530 sh. ESI-MS, *m/z* Found (Calcd) = 1565.85 (1565.07) $[(Ph)_4P][Fe(I_2An)_3]-H]^-$; 781.90 (782.42) $[(Ph)_4P][Fe(I_2An)_3]^{2-}$.

Characterization

FT-IR spectra were performed on KBr pellets and collected with a Bruker Equinox 55 spectrophotometer. Electronic spectra (1200–200 nm) were recorded in CH₃CN solution on a Varian Cary 5 spectrophotometer. C, H, N analyses were performed with a Thermo Electron Analyzer CHNS Flash 2000 or with a Carlo Erba mod. EA1108 CHNS analyzer. ESI-MS spectra were collected on a Bruker Esquire 3000 Ionic Trap (TOF analyzer) in negative and positive mode.

Cyclic Voltammetry

Cyclic voltammetry was carried out on a BioLogic potentiostat model SP-150, using a three-electrode cell equipped with a platinum millielectrode with a surface area of 0.126 cm², an Ag/Ag⁺ pseudoreference and a platinum-wire as counterelectrode. The experiments were performed at room temperature (25 °C), in dry and Nitrogen-degassed CH₃CN solution containing 0.1 mol dm⁻³ $[(n-Bu)_4N]PF_6$ as supporting electrolyte, at 50 mV s⁻¹ scan rate. All the voltamograms were corrected for the half-wave potential of the ferrocene-ferrocenium couple as internal standard (0.42 V under these conditions).

Single Crystal X-Ray Crystallography

A summary of data collection and structure refinement for **1c**, **2c**, **5a**, **2b**, **4b**, **6b**, are reported in Table 3.

Table 3 Summary of X-ray crystallographic data for **1c**, **2c**, **5a**, **2b**, **4b**, **6b**.

	1c	2c	5a	2b	4b	6b
Empirical formula	C ₃₆ H ₅₀ Cl ₆ CrN ₃ O ₁₄	C ₃₆ H ₅₀ Cl ₆ FeN ₃ O ₁₄	C ₆₆ H ₁₀₈ CrI ₆ N ₃ O ₁₂	C ₉₀ H ₆₂ Cl ₆ FeO ₁₃ P ₃	C ₉₀ H ₆₂ Br ₆ FeO ₁₃ P ₃	C ₉₀ H ₆₈ I ₆ FeO ₁₆ P ₃
Formula weight	997.49	1019.36	1948.95	1712.86	1979.62	2311.57
Colour, habit	Red, block	Black, block	Red, plate	Dark red, needle	Dark red, plate	Dark red, plate
Crystal size, mm	0.27x0.15x0.10	0.33x0.27x0.13	0.14x0.09x0.05	0.19x0.03x0.03	0.12x0.08x0.03	0.29x0.24x0.07
Crystal system	Monoclinic	Orthorhombic	Orthorhombic	Monoclinic	Monoclinic	Monoclinic
Space group	<i>P</i> 2 ₁ / <i>n</i>	<i>P</i> bcn	<i>P</i> bca	<i>P</i> 2 ₁ / <i>n</i>	<i>P</i> 2 ₁ / <i>n</i>	<i>C</i> 2/ <i>c</i>
<i>a</i> , Å	16.154(3)	26.340(6)	24.339(1)	13.336(3)	13.408(2)	35.023(5)
<i>b</i> , Å	10.575(2)	16.510(4)	20.262(1)	18.855(5)	18.871(2)	12.482(2)
<i>c</i> , Å	26.682(4)	10.564(3)	32.155(2)	32.473(8)	32.851(4)	46.347(7)
α , deg.	90	90	90	90	90	90
β , deg.	92.092(3)	90	90	91.462(4)	91.198(3)	114.467(2)
γ , deg.	90	90	90	90	90	90
<i>V</i> , Å ³	4555(1)	4594(2)	15858(1)	8163(3)	8310(2)	18441(5)
<i>Z</i>	4	4	8	4	4	8
<i>T</i> , K	293(2)	293(2)	293(2)	293(2)	293(2)	293(2)
ρ (calc), Mg/m ³	1.455	1.474	1.633	1.394	1.582	1.665
μ , mm ⁻¹	0.665	0.742	2.534	0.504	3.187	2.286
θ range, deg.	1.45 to 27.58	1.46 to 27.08	1.45 to 24.00	1.25 to 23.33	1.24 to 22.81	1.75 to 23.42
No. of rflcn/obsv	53418 / 10212	38219 / 5042	152710 / 12407	74863 / 11760	36597 / 11167	36675 / 13255
GooF	1.007	1.020	1.064	1.015	1.003	1.042
<i>R</i> 1	0.0834	0.0572	0.0570	0.0887	0.0735	0.0894
<i>wR</i> 2	0.1515	0.1562	0.1206	0.1592	0.1123	0.1518

$$R1 = \frac{\sum |F_o| - |F_c|}{\sum |F_o|}, wR2 = \frac{[\sum [w(F_o^2 - F_c^2)^2] / \sum [w(F_o^2)^2]]^{1/2}}{w}, w = 1 / [\sigma^2(F_o^2) + (aP)^2 + bP], \text{ where } P = [\max(F_o^2, 0) + 2F_c^2] / 3.$$

Single crystal data were collected with a Bruker AXS Smart 1000 and with a Bruker Smart APEXII area detector diffractometers. All data collection were performed with the Mo K α radiation ($\lambda = 0.71073$ Å). Cell constants were obtained using 60 ω -frames of 0.5° width and scanned from three different zone of reciprocal lattice. The intensity data were integrated from several series of exposures frames of 0.3° width.¹⁸ Absorption corrections were applied using the program SADABS.¹⁹ The structures were solved by direct methods (SIR97 and SIR2004^{20,21}) and refined on F^2 with full-matrix least squares (SHELXL-97²²), using the Wingx software package.²³ The crystallization water molecules were refined without the hydrogen atoms. The crystals of **2b** and **4b** were thin plates and diffracted poorly, and only a partial structure determination could be obtained. These two structures are nonetheless described for comparison purposes. In **2b** and **4b** the carbon atoms of the PPh₄⁺ cations were refined with isotropic displacement parameters, and one of the ligands was found disordered in two positions that were refined with isotropic thermal parameters and with site occupancy factors of

0.53/0.47 and 0.62/0.38, respectively. The remaining non hydrogen atoms were refined anisotropically for all compounds, and the hydrogen atoms were placed at their calculated positions. Graphical material was prepared with the ORTEP3 for Windows²⁴ and Mercury CSD 3.0²⁴ programs. CCDC 941114, 941115, 941116, 941119 contain the supplementary crystallographic data for the reported compounds.

Powder X-Ray Crystallography

Wide-Angle X-Ray Diffraction (WAXRD) patterns on microcrystalline powder samples were recorded on a Panalytical Empyrean diffractometer equipped with a graphite monochromator on the diffracted beam, and a X'Celerator linear detector. The scans were collected within the range 5–40° (2θ) using Cu K α radiation. The simulated patterns were generated from the atomic coordinates of the single-crystal structure solutions using the program Mercury 3.1 (copyright CCDC, <http://www.ccdc.cam.ac.uk/mercury/>) using a FWHM (full width at half maximum) of 0.15 and a 2θ step of 0.05.

Computational details

Density functional theory calculations were performed on the isolated anions X_2An ($X = Cl, Br, I$) and on the complexes $[M(X_2An)_3]^{3-}$ ($M = Fe(III), Cr(III)$; $X = Cl, Br, I$). The geometries of the anions were optimized with the B3LYP^{25,26} hybrid density functional and the SDD basis set with Stuttgart-Dresden effective core potential for bromine and iodine atoms.²⁷⁻²⁹ The geometries of the metal complexes were optimized with the B3LYP density functional and the LANL2DZ basis set with Hay and Wadt effective core potential (ECP)^{30,31} for iron, chromium and halogen atoms and the 6-31G basis set^{32,33} for the C and O atoms. Single point calculations were performed on the complexes by using the B3LYP density functional and the LANL2DZ basis set with Hay and Wadt ECP for the metal ions and halogen atoms, whereas C and O atoms were treated with the 6-31+G(d) basis set. Atomic charges derived by the natural population analysis (NPA) were obtained with the NBO 3.1 program³⁴ incorporated in the Gaussian03 package. Molecular orbital diagrams and electrostatic potential diagrams were generated with the MOLDEN program.³⁵ All the calculations have been performed with the Gaussian03 program suite.³⁶

Magnetic Properties

The magnetic susceptibility measurements were performed with a Quantum Design MPMS-XL-5 SQUID susceptometer in the temperature range 2–300 K with an applied magnetic field of 0.1 or 0.5 T on polycrystalline samples of compounds **1-6** with masses of 22.04, 15.36, 20.22, 21.52, 20.96, 23.17, 22.48, 15.67, 18.05, 11.66, 24.97, 18.34, 26.00, 11.38 mg for **1a**, **1b**, **1c**, **2a**, **2b**, **2c**, **3a**, **3b**, **4a**, **4b**, **5a**, **5b**, **6a**, **6b**, respectively. The isothermal magnetization measurements were performed on the same samples at 2 K with magnetic fields up to 5 T with the same equipment. The susceptibility data were corrected for the sample holder previously measured using the same conditions and for the diamagnetic contributions of the salt using Pascal's constant tables.³⁷ Powder XRD (PXRD) measurements have been performed on the same microcrystalline samples that were measured in the SQUID and they show experimental patterns which correspond to the simulated X-Ray patterns obtained from the single crystal X-Ray structures. PXRD data are reported in the Supporting Information (Figures S5-S7, S11-S12).

Conclusions

The preparation through a novel general synthetic strategy of six new $[M^{III}(X_2An)_3]^{3-}$ ($M^{III} = Cr, Fe$; $X = Cl, Br, I$) tris(haloanilato)metallate(III) complexes, and their crystal structures, spectroscopic characterization, DFT calculations, and magnetic properties are reported. These complexes represent a new family of anionic building blocks where halogens play a key role in determining the physical properties of the resulting materials, either at the electronic level, by varying the electron density on the anilate ring, or at the supramolecular level, affecting the molecular packing via

halogen-bonding interactions. Especially compounds **3-6** represent one of the few examples of metal complexes with bromanilato and iodanilato ligands reported in the literature. It is noteworthy that the presence of halogen-bonding interactions in **5a** are responsible for a unique magnetic behaviour in this family; this complex shows antiferromagnetic interactions among metal ions, with an antiferromagnetic transition at 4.1(1) K, in agreement with the formation of halogen-bonded supramolecular dimers. Furthermore, as perspective, this family of anionic complexes, which have shown to be excellent candidates for constructing 2D molecule-based ferrimagnets with tunable ordering temperature as a function of the halogen electronegativity¹⁰, can work *i)* as precursors for the preparation of metal-organic frameworks with tunable size which depends, in turn, on the halogen size; *ii)* as magnetic components for building up multifunctional molecular materials based on BEDT-TTF organic donors which furnish the pathway for combining electrical conductivity with magnetic properties, in analogy with the relevant class of $[M(ox)_3]^{3-}$ ($ox = oxalate$) trischelated complexes which have produced the first family of molecular paramagnetic superconductors.³⁸

Acknowledgements

This work is supported by Regione Autonoma della Sardegna, L.R. 7-8-2007, Bando 2009, CRP-17453 Project “Nano Materiali Multifunzionali per Applicazioni nell’Elettronica Molecolare”, Fondazione Banco di Sardegna and INSTM. Work in France was supported by the CNRS and University of Angers. Prof. Carlos Gómez-García and Dr. Samia Benmansour are kindly acknowledged for magnetic measurements. Dr. Ingrid Freuze is acknowledged for ESI-MS analyses.

Notes and references

† Dipartimento di Scienze Chimiche e Geologiche, Università degli Studi di Cagliari, S.S. 554 – Bivio per Sestu – I09042 Monserrato (Cagliari), Italy;

‡ Dipartimento di Chimica, Università di Parma, Parco Area delle Scienze 17A, I-43124 Parma, Italy;

§ Dipartimento di Fisica, Università degli Studi di Cagliari, S.S. 554 – Bivio per Sestu – I09042 Monserrato (Cagliari), Italy;

◇ Université d’Angers, CNRS UMR 6200, Laboratoire MOLTECH-Anjou 2 bd Lavoisier, 49045 Angers, France.

† Electronic Supplementary Information (ESI) available: additional Ortep drawings, FT-IR spectra, PXRD patterns, additional susceptibility measurements, Cyclic Voltammetry data. See DOI: 10.1039/b000000x/. CCDC 941114 - 941119 contain the supplementary crystallographic data for this paper. These data can be obtained free of charge from The Cambridge Crystallographic Data Centre via www.ccdc.cam.ac.uk/data_request/cif.

- (a) P. Metrangolo, F. Meyer, T. Pilati, G. Resnati, G. Terraneo, *Angew. Chem. Int. Ed.*, 2008, **47**, 6114-6127; (b) M. Fourmigué, *Curr. Opin. Solid State Mater. Sci.*, 2009, **13**, 36-45; (c) P. Politzer, J. S. Murray, T. Clark, *Physical Chemistry Chemical Physics*, 2010, **12**, 7748.

- 2 (a) D. Braga, L. Maini, M. Polito, F. Grepioni, *Structure and Bonding*, 2004, **111**, 1-32; (b) R. Vilar, *Structure and Bonding*, 2004, **111**, 85-137; (c) V. A. Russell, C. C. Evans, W. Li, M. D. Ward, *Science*, 1997, **276**, 575-579; (d) G. R. Desiraju, *J. Am. Chem. Soc.*, 2013, **135**, 9952-9967; (e) M. Atzori, E. Sessini, F. Artizzu, L. Pilia, A. Serpe, C. J. Gómez-García, C. Giménez-Saiz, P. Deplano, M. L. Mercuri, *Inorg. Chem.*, 2012, **51**, 5360-5367.
- 3 T. Imakubo, H. Sawa, R. Kato, *Synth. Met.*, 1995, **73**, 117.
- 4 (a) M. Fourmigué, P. Batail, *Chem. Rev.*, 2004, **104**, 5379-5418; (b) M. Fourmigué, *Struct. Bond.*, 2008, **126**, 181-207.
- 5 S. Kitagawa, S. Kawata, *Coord. Chem. Rev.*, 2002, **224**, 11-34.
- 6 (a) M. Kawahara, M. K. Kabir, K. Yamada, K. Adachi, H. Kumagai, Y. Narumi, K. Kindo, S. Kitagawa, S. Kawata, *Inorg. Chem.*, 2004, **43**, 92-100; (b) K. Heinze, G. Huttner, L. Zsolnai, A. Jacobi, P. Schober, *Eur. J. Inorg. Chem.*, 1997, **3**, 732-743; (c) C. Fujii, M. Mitsumi, M. Kodera, K.-I. Motoda, M. Ohba, N. Matsumoto, H. Okawa, *Polyhedron* 1994, **13**, 933-938.
- 7 (a) B. F. Abrahams, M. J. Grannas, T. A. Hudson, S. A. Hughes, N. H. Pranoto, R. Robson, *Dalton Trans.*, 2011, **40**, 12242; (b) B. F. Abrahams, T. A. Hudson, L. J. McCormick, R. Robson, *Cryst. Growth Des.*, 2011, **11**, 2717-2720; (c) T. Luo, Y. Liu, H. Tsai, C. Su, C. Ueng, K. Lu, *Eur. J. Inorg. Chem.*, 2004, 4253-4258; (d) B. F. Abrahams, J. Coleiro, K. Ha, B. F. Hoskins, S. D. Orchard, R. Robson, *J. Chem. Soc. Dalton Trans.*, 2002, 1586-1594; (e) S. Kawata, S. Kitagawa, H. Kumagai, T. Ishiyama, K. Honda, H. Tobita, K. Adachi, M. Katada, *Chem. Mater.*, 1998, **10**, 3902-3912; (f) S. Decurtins, H. W. Schmalle, L. M. Zheng, J. Ensling, *Inorg. Chim. Acta*, 1996, **244**, 165-170.
- 8 (a) M. K. Kabir, N. Miyazaki, S. Kawata, K. Adachi, H. Kumagai, K. Inoue, S. Kitagawa, K. Iijima, M. Katada, *Coord. Chem. Rev.*, 2000, **198**, 157-169; (b) K. Molčanov, M. Jurić, B. Kojić-Prodić; *Dalton Trans.*, 2013, **42**, 15756.
- 9 K. S. Min, A. L. Rhinegold, J. S. Miller, *J. Am. Chem. Soc.*, 2006, **128**, 40-41.
- 10 M. Atzori, S. Benmansour, G. Mínguez Espallargas, M. Clemente-León, A. Abhervé, P. Gómez-Claramunt, E. Coronado, F. Artizzu, E. Sessini, P. Deplano, A. Serpe, M. L. Mercuri, C. J. Gómez-García, *Inorg. Chem.*, 2013, **52**, 10031-10040.
- 11 C.J. Cramer, *Essentials of Computational Chemistry. Theories and Models*, 2nd ed., 2004, John Wiley & Sons, Chichester, UK.
- 12 E. Scrocco, J. Tomasi, The electrostatic molecular potential as a tool for the interpretation of molecular properties. *Top. Curr. Chem.*, 1973, **42**, 95.
- 13 E. Ruiz, J. Cirera, S. Alvarez, *Coordination Chemistry Reviews*, 2005, **249**, 2649-2660.
- 14 A. Pawlukojć, G. Bator, L. Sobczyk, E. Grech, J. Nowicka-Scheibe, *Journal of Physical Organic Chemistry*, 2003, **16**, 709.
- 15 (a) C. J. O'Connor, *Prog. Inorg. Chem.*, 1982, **29**, 203; (b) O. Kahn, *Molecular Magnetism*, 1993, VCH Publishers, Cambridge, UK, p. 9; (c) A. H. Morrish, *The Physical Principles of Magnetism*, 2001, IEEE Press, New York, US, p. 432.
- 16 (a) M. Fourmigué, *Structure and Bonding*, Springer-Verlag: Berlin, 2008, **126**, 181; (b) X. Pang, X. R. Zhao, H. Wang, H.L. Sun, W. Jun Jin, *Cryst. Growth Des.*, 2013, **13**, 3739; (c) T. R. Butcher, J. J. Novoa, J. Ribas-Ariño, A. W. Sandvik, M. M. Turnbull, C. P. Landee, M. B. Wells, F. F. Awwadi, *Chem. Commun.*, 2009, 1359-1361; (d) J. A. Schlueter, H. Park, G. J. Halder, W. R. Armand, C. Dunmars, K. W. Chapman, J. L. Manson, J. Singleton, R. McDonald, A. Plonczak, J. Kang, C. Lee, M. H. Whangbo, T. Lancaster, A. J. Steele, I. Franke, J. D. Wright, S. J. Blundell, F. L. Pratt, J. de George, M. M. Turnbull, C. P. Landee, *Inorg. Chem.*, 2012, **51**, 2121-2129.
- 17 (a) H. A. Torrey, W. H. Hunter, *J. Am. Chem. Soc.*, 1912, **34**, 702. (b) J. Stenhouse, *J. Chem. Soc.*, 1870, **23**, 6-14.
- 18 SMART (control) and SAINT (integration) software for CCD systems, Bruker AXS, Madison, WI, USA, 1994.
- 19 Area-Detector Absorption Correction, Siemens Industrial Automation Inc., Madison, WI, 1996
- 20 A. Altomare, M. C. Burla, M. Camalli, G. L. Casciarano, C. Giacovazzo, A. Guagliardi, A. G. G. Moliterni, G. Polidori, R. Spagna, SIR97: a new tool for crystal structure determination and refinement. *Journal of Applied Crystallography*, 1999, **32**, 115-119.
- 21 M. C. Burla, R. Caliendo, M. Camalli, B. Carrozzin, G. L. Casciarano, L. De Caro, C. Giacovazzo, G. Polidori, R. Spagna, SIR2004: an improved tool for crystal structure determination and refinement 35. *Journal of Applied Crystallography*, 2005, **38**, 381-388.
- 22 G. M. Sheldrick, SHELX97. Programs for Crystal Structure Analysis (1997) (Release 97-2). University of Göttingen, Germany.
- 23 L. J. Farrugia, WinGX suite for small-molecule single-crystal crystallography. *Journal of Applied Crystallography*, 1999, **32**, 837-838.
- 24 C. F. Macrae, P. R. Edgington, P. McCabe, E. Pidcock, G. P. Shields, R. Taylor, M. Towler, J. van de Streek, *J. Appl. Crystallogr.*, 2006, **39**, 453-457.
- 25 A. D. Becke, Density-functional exchange-energy approximation with correct asymptotic behavior. *Physical Review A: Atomic, Molecular, and Optical Physics*, 1988, **38**, 3098-3100.
- 26 A. D. Becke, Density-Functional Thermochemistry 3. the Role of Exact Exchange. *Journal of Chemical Physics*, 1993, **98**, 5648-5652.
- 27 P. Fuentealba, H. Preuss, H. Stoll, and L. v. Szentpaly, *Chem. Phys. Lett.*, 1989, **89**, 418.
- 28 X. Y. Cao and M. Dolg, *J. Mol. Struct. (Theochem)*, 2002, **81**, 139.
- 29 P. Schwerdtfeger, M. Dolg, W. H. E. Schwarz, G. A. Bowmaker, and P. D. W. Boyd, *J. Chem. Phys.*, 1989, **91**, 1762.
- 30 P. J. Hay, W. R. Wadt, *Journal of Chemical Physics*, 1985, **82**, 299-310.
- 31 W. R. Wadt, P. J. Hay, *Journal of Chemical Physics*, 1985, **82**, 284-298.
- 32 R. Ditchfield, W. J. Hehre, and J. A. Pople, *J. Chem. Phys.*, 1971, **54**, 724
- 33 V. A. Rassolov, M. A. Ratner, J. A. Pople, P. C. Redfern, and L. A. Curtiss, *J. Comp. Chem.*, 2001, **22**, 976.
- 34 *NBO version 3.1*, E.D. Glendening, A.E. Reed, J.E. Carpenter, F. Weinhold, 2013.
- 35 G. Schaftenaar and J.H. Noordik, *J. Comput.-Aided Mol. Design*, 2000, **14**, 123-134.
- 36 Gaussian 03, Revision C.02, M. J. Frisch, G. W. Trucks, H. B. Schlegel, G. E. Scuseria, M. A. Robb, J. R. Cheeseman, Jr. J. A. Montgomery, T. Vreven, K. N. Kudin, J. C. Burant, J. M. Millam, S. S. Iyengar, J. Tomasi, V. Barone, B. Mennucci, M. Cossi, G.

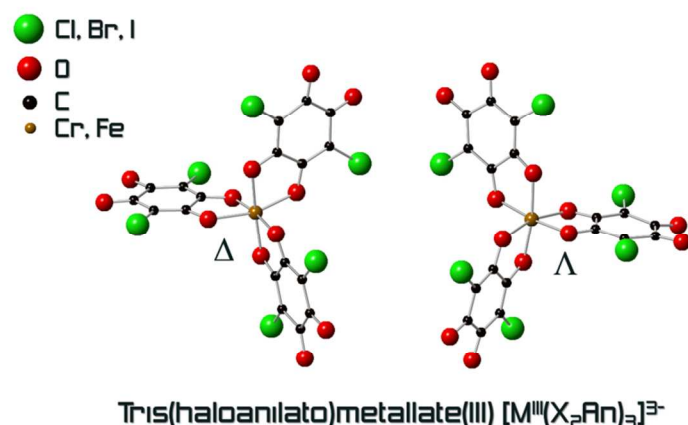
Scalmani, N. Rega, G. A. Petersson, H. Nakatsuji, M. Hada, M. Ehara, K. Toyota, R. Fukuda, J. Hasegawa, M. Ishida, T. Nakajima, Y. Honda, O. Kitao, H. Nakai, M. Klene, X. Li, J. E. Knox, H. P. Hratchian, J. B. Cross, V. Bakken, C. Adamo, J. Jaramillo, R. Gomperts, R. E. Stratmann, O. Yazyev, A. J. Austin, R. Cammi, C. Pomelli; J. W. Ochterski, P. Y. Ayala, K. Morokuma, G. A. Voth, P. Salvador, J. J. Dannenberg, V. G. Zakrzewski, S. Dapprich; A. D. Daniels, M. C. Strain, O. Farkas, D. K. Malick, A. D. Rabuck, K. Raghavachari, J. B. Foresman, J. V. Ortiz, Q. Cui, A. G. Baboul, S. Clifford, J. Cioslowski, B. B. Stefanov, G. Liu, A. Liashenko, P. Piskorz, I. Komaromi, R. L. Martin, D. J. Fox, T. Keith, M. A. Al-

Laham, C. Y. Peng, A. Nanayakkara, M. Challacombe, P. M. W. Gill, B. Johnson, W. Chen, M. W. Wong, C. Gonzalez, and J. A. Pople, *Gaussian, Inc.*, Wallingford CT, 2004.

37 G. A. Bain, J. F. Berry, *J. Chem. Educ.*, 2008, **85**, 532.

38 (a) M. Kurmoo, A. W. Graham, P. Day, S.J. Coles, M.B. Hursthouse, J. M. Caulfield, J. Singleton, L. Ducasse, P. Guionneau, *J. Am. Chem. Soc.*, 1995, **117**, 12209; (b) E. Coronado, P. Day, *Chem. Rev.*, 2004, **104**, 5419; (c) M. L. Mercuri, P. Deplano, A. Serpe, F. Artizzu, *Multifunctional Materials of interest in Molecular Electronics*, Chapter in *Handbook of Multifunctional Molecular Materials*, Ouahab, L., ed.; Pan Stanford Publishing, 2011.

Graphical Abstract



Here we report on new tris(haloanilato)metallate(III) complexes with general formula $[M(X_2An)_3]^{3-}$ ($M(III) = Cr, Fe$; $X = Cl, Br, I$; $An = anilate$), their crystal structures, DFT calculations and magnetic properties.